



# Incorporation of iron and organic matter into young Antarctic sea ice during its initial growth stages

Julie Janssens<sup>1,2,3\*</sup> • Klaus M. Meiners<sup>2,3</sup> • Jean-Louis Tison<sup>4</sup> • Gerhard Dieckmann<sup>5</sup> • Bruno Delille<sup>6</sup> • Delphine Lannuzel<sup>1,2</sup>

<sup>1</sup>Institute for Marine and Antarctic Studies, University of Tasmania, Hobart, Tasmania, Australia

<sup>2</sup>Antarctic Climate and Ecosystems Cooperative Research Centre, University of Tasmania, Hobart, Tasmania, Australia

<sup>3</sup>Australian Antarctic Division, Department of the Environment, Kingston, Tasmania, Australia

<sup>4</sup>Glaciology Unit, Department of Earth and Environmental Science, Université Libre de Bruxelles, Bruxelles, Belgium

<sup>5</sup>Alfred-Wegener-Institut Helmholtz-Zentrum für Polar und Meeresforschung, Bremerhaven, Germany

<sup>6</sup>Unité d'Océanographie Chimique, MARE, Université de Liège, Liège, Belgium

\*Julie.Janssens@utas.edu.au

## Abstract

This study reports concentrations of iron (Fe) and organic matter in young Antarctic pack ice and during its initial growth stages *in situ*. Although the importance of sea ice as an Fe reservoir for oceanic waters of the Southern Ocean has been clearly established, the processes leading to the enrichment of Fe in sea ice have yet to be investigated and quantified. We conducted two *in situ* sea-ice growth experiments during a winter cruise in the Weddell Sea. Our aim was to improve the understanding of the processes responsible for the accumulation of dissolved Fe (DFe) and particulate Fe (PFe) in sea ice, and of particulate organic carbon and nitrogen, dissolved organic carbon, extracellular polymeric substances, inorganic macro-nutrients (silicic acid, nitrate and nitrite, phosphate and ammonium), chlorophyll *a* and bacteria. Enrichment indices, calculated for natural young ice and ice newly formed *in situ*, indicate that during Antarctic winter all of the measured forms of particulate matter were enriched in sea ice compared to underlying seawater, and that enrichment started from the initial stages of sea-ice formation. Some dissolved material (DFe and ammonium) was also enriched in the ice but at lower enrichment indices than the particulate phase, suggesting that size is a key factor for the incorporation of impurities in sea ice. Low chlorophyll *a* concentrations and the fit of the macro-nutrients (with the exception of ammonium) with their theoretical dilution lines indicated low biological activity in the ice. From these and additional results we conclude that physical processes are the dominant mechanisms leading to the enrichment of DFe, PFe, organic matter and bacteria in young sea ice, and that PFe and DFe are decoupled during sea-ice formation. Our study thus provides unique quantitative insight into the initial incorporation of impurities, in particular DFe and PFe, into Antarctic sea ice.

## 1. Introduction

It is now well established that sea ice represents an important reservoir of iron (Fe) to the Fe-depleted waters of the Southern Ocean (e.g., Sedwick and DiTullio, 1997; Lancelot et al., 2009; Lannuzel et al., 2010; Wang et al., 2014). The seasonal cycle of sea-ice formation and retreat in Antarctica affects approximately 40% of the entire Southern Ocean and impacts the whole Antarctic ecosystem (Arrigo, 2014). During formation, sea ice has a generally low capacity to incorporate salts and impurities such as biotic or abiotic particles and dissolved components (Cox and Weeks, 1975). The growing sea-ice crystals reject impurities into the liquid brine found within the ice. Small amounts of seawater can be trapped in the advancing ice interface, entraining some impurities, but most of the seawater is rejected at the ice-seawater interface. However, Antarctic field studies have shown Fe and organic matter enrichment of 1 to 2 orders of magnitude over seawater (Grotti et al., 2005; Lannuzel et al., 2007, 2008, 2014a, 2014b; van der Merwe et al., 2009, 2011a, 2011b; de Jong et al.,

### Domain Editor-in-Chief

Jody W. Deming,  
University of Washington

### Associate Editor

Lisa A. Miller,  
Fisheries and Oceans Canada

### Knowledge Domain

Ocean Science

### Article Type

Research Article

### Part of an *Elementa* Special Feature

Biogeochemical Exchange Processes at Sea-Ice Interfaces (BEPsII)

Received: October 16, 2015

Accepted: July 10, 2016

Published: August 18, 2016

2013, 2015). The co-occurrence of high concentrations of Fe and organic matter in the ice suggests coupled processes leading to their enrichment (Lannuzel et al., 2007, 2015; Schoemann et al., 2008). Specifically, van der Merwe et al. (2009) proposed that Fe can be associated with extracellular polymeric substances (EPS) and co-incorporated into the ice.

A combination of biological and physical mechanisms could explain incorporation of biogenic and lithogenic materials into sea ice. These mechanisms include: (1) sediment entrapment in newly formed sea ice (e.g., Nürnberg et al., 1994; Lindemann et al., 1997; Lindemann, 1998; Smedsrud, 1998; Dethleff and Kempema, 2007; Dethleff and Kuhlmann, 2009); (2) dissolved macro-nutrient entrapment (Riedel et al., 2007; Zhou et al., 2014); (3) dissolved organic matter entrapment (e.g., Giannelli et al., 2001; Ewert and Deming, 2011; Müller et al., 2013); and (4) entrapment of particulate biogenic material (e.g., Garrison et al., 1989; Gradinger and Ikävalko, 1998; Weissenberger and Grossmann, 1998; Róžańska et al., 2008).

The proposed processes for incorporation of particulate impurities into sea ice are as follows. When the first crystals of frazil ice form in the water column, they are thought to harvest or scavenge the particulate matter present in the water column during their rise to the surface (Weeks and Ackley, 1982; Osterkamp and Gosink, 1983; Garrison et al. 1989; Reimnitz et al., 1993; Dethleff, 2005). Microorganisms and detritus can act as nucleation sites for the ice crystals (Weeks and Ackley, 1982; Knopf et al., 2011). Once particles associated with frazil ice crystals have accumulated in the surface water, they can be concentrated under the action of Langmuir circulation cells and trapped in newly forming ice (Martin and Kauffman, 1981). Although this process has not been particularly well studied in Antarctica, it is considered to be a leading mechanism in the formation of sediment-laden sea ice in the Arctic (Dethleff, 2005; Dethleff and Kempema, 2007; Dethleff et al., 2009). Young Arctic sea ice with high sediment content also contains high dissolved metal concentrations, including dissolved Fe (Hölemann et al., 1997). Similarly, the suspended material can be concentrated by wave-field pumping passing through the freshly formed layer of frazil ice (Lindemann et al., 1997). These particles then become attached to, or trapped in or between, the ice crystals (Weissenberger and Grossmann, 1998). Once a layer of ice isolates the water from the atmosphere, thermodynamic ice-growth processes dominate, and congelation ice starts to form. When congelation ice grows, exchange of sea salts and macro-nutrients between seawater and ice are controlled by convective fluid movement induced by strong salinity gradients across the ice-water interface (e.g., Vancoppenolle et al., 2010). These convective movements could be responsible for the aggregation at the seawater/sea-ice boundary of living and dead microorganisms, which then can become incorporated into the sea ice as the ice continues to grow (Lannuzel et al., 2010). The organic matter observed in columnar ice could alternatively originate from *in situ* biological processes; e.g., algal growth within the ice cover (Lizotte, 2003). Bio-accumulation through ice algal growth was suggested by Spindler (1994) as a key driver of high concentrations of organic matter (living and dead) in columnar ice. Because organic matter contains Fe, this bioaccumulation mechanism would lead to the incorporation of Fe in sea ice together with organic matter.

Due to the varying processes involved in sea-ice formation, frazil ice should theoretically be more enriched in Fe and organic matter than columnar ice, which forms more slowly and therefore expels impurities more effectively. However, this rationale only relies on initial incorporation processes and does not take into account *in situ* biogeochemical, transport and other processes. To date, no relationship between Fe content and ice texture has been clearly established (Lannuzel et al., 2007, 2014a; van der Merwe et al., 2009), and the relationships between sea-ice formation and the Fe cycle in surface polar oceans remain poorly understood.

The aim of this study was to investigate the potential occurrence and pathways of Fe and organic matter enrichment in newly formed sea ice during two *in situ* time-series ice-growth experiments in the Weddell Sea during austral winter. We also explored the entrapment signature in different types of young sea ice collected opportunistically during the voyage. To our knowledge, this study is the first attempt to investigate the initial pathways leading to Fe enrichment in Antarctic sea ice.

## 2. Methods

### 2.1 Cleaning procedures for trace metal work

All sampling bottles (Nalgene, of low-density polyethylene, LDPE), melting containers (polypropylene, PP) and equipment were cleaned following the GEOTRACES recommendations (Cutter et al., 2010). In short, they were immersed for one week in 2% (v:v) Decon90 and then rinsed four times with reverse osmosis water (ROW) and three times with ultra high purity water (UHP water, Barnstead International, NANO-pure Diamond polisher) before being soaked in a 50% (v:v) HCl bath (analytical grade Merck EMSURE, Germany) for one month. Bottles were then rinsed five times with UHP water in a class-100 laminar flow hood before being filled with 10% (v:v) HCl (Ultrapure, Seastar Baseline) and triple-bagged until used on the voyage. Before use, bottles were rinsed three times with UHP water and three times with the sample. During the voyage, filtration sets and other plastic equipment (Teflon filtration set, tubing, scoop, PP melting containers, etc.) were immersed in 20% (v:v) HCl between stations. Equipment used for Fe filtrations was thoroughly rinsed with UHP water, 10% (v:v) HCl and UHP water between the processing of the samples.

## 2.2 Sampling area

Sea-ice early growth experiments and young ice sampling were conducted during the Antarctic Winter Ecosystem and Climate Study (AWECS/ANT-XXIX/6) voyage with RV *Polarstern* to the Weddell Sea in June–August 2013 (Lemke et al., 2014; Figure 1). The first time-series ice-growth experiment (Station 506) started on 12 July 2013 in the middle of the Weddell Sea and ended on 14 July 2013. The second experiment (Station 517) was performed closer to the Antarctic Peninsula and the continental shelf between 29 and 31 July 2013 (Table 1). Natural young ice was also collected at five other stations (Stations 486–500; Figure 1).

Table 1. Young ice sampling locations and physical parameters

Station Number	Location	Sampling date, 2013	Type of ice	Sampling method	Snow thickness (m)	Ice thickness (m)	Ice temperature (°C)	Bulk ice salinity (S <sub>p</sub> ) <sup>a</sup>	V <sub>b</sub> /V (%) <sup>b</sup>
486	61°31 S, 00°05 W	17 June	Unconsolidated pancake	Cage + gloved hands	No snow	0.06–0.07	–5.0	23.7	26
488	62°54 S, 00°00 W	18 June	Semi-consolidated pancake	Cage + TM corer	<0.01	0.30–0.36	–4.1	5.3	6
489	63.54° S, 00.01° W	19 June	Consolidated pancake	Cage + TM corer	0.03	0.30–0.36	–3.4	6.3	9
496	67.26° S, 00°01 W	24 June	Thin ice	Kovacs corer + Ti-coated handsaw	0.04	0.42–0.46	–3.2	8.3	13
500	67°57 S, 06°39 W	05 July	Grey ice	Ti-coated handsaw	No snow	0.05–0.06	–3.3	18.5	28
506	67°11 S, 23°00 W	12–14 July	<i>In situ</i> Exp 1	Ti-coated handsaw + TM corer	Snow removed	See Table 2	See Table 2	See Table 2	See Table 2
517	63°34 S, 51°10 W	29–31 July	<i>In situ</i> Exp 2	Ti-coated handsaw + TM corer	Snow removed	See Table 2	See Table 2	See Table 2	See Table 2

<sup>a</sup>Seawater salinity (S<sub>p</sub>) was 34.2, 34.5, 34.8, 34.2, and 34.2 at stations 486, 488, 489, 496, and 500, respectively.

<sup>b</sup>V<sub>b</sub>/V = Brine volume fraction

doi: 10.12952/journal.elementa.000123.t001

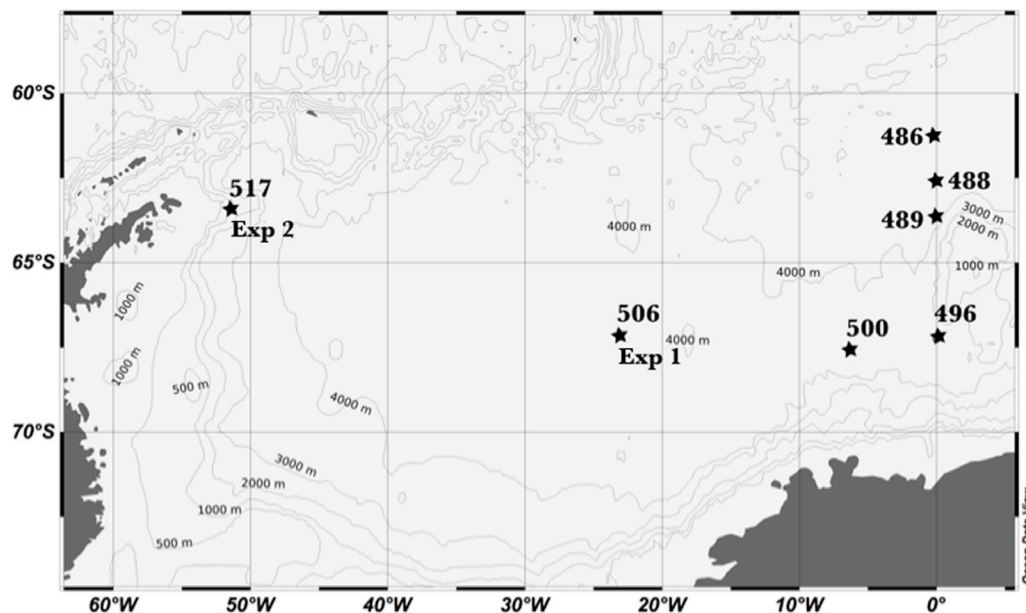


Figure 1  
Sampling location.

Locations of the young ice sampling stations (Stations 486, 488, 489, 496 and 500) and the two *in situ* ice-growth time-series experiments (Stations 506 and 517 for Experiments 1 and 2, respectively) of the AWECS cruise in the Weddell Sea during June–August 2013. Note that only the stations pertaining to this dataset are shown.

doi: 10.12952/journal.elementa.000123.f001

### 2.3 *In situ* ice-growth time-series experiments

Experiments were conducted in areas of level ice, upwind from the ship and other activities on the ice to avoid contamination. Prior to ice coring, snow was removed using an acid-clean plastic shovel. Collection and processing of ice and water samples were conducted using the methods outlined by Lannuzel et al. (2006). Seawater was collected from the ice-water interface using a peristaltic pump (E/S Portable Sampler, Masterflex) equipped with acid-clean silicon tubes. For each experiment, four rows of holes (Figure 2) were drilled through the ice using a trace metal (TM) clean electro-polished stainless steel ice corer previously tested for TM sampling (14 cm internal diameter, Lichtert Industry, Belgium; Lannuzel et al., 2006). Each row corresponds to an increasing time step and each core (A to F, Figure 2) was allocated to measure one of the parameters described below. Holes were cleared of coring debris and slush with an acid-clean plastic scoop, which denoted the start of an experiment ( $T_0 = 0$  h). Ice was then allowed to grow in each hole and subsequently collected at increasing time steps ( $T_1 = 6$  h,  $T_2 = 12$  h,  $T_3 = 24$  h and  $T_4 = 48$  h). The  $T_1$  samples were collected using a titanium (Ti)-coated handsaw (Claus Titanium). Titanium is a material commonly used for trace metal sampling (de Baar et al., 2008; Cutter et al., 2010).  $T_2$ ,  $T_3$  and  $T_4$  rows were collected using the TM-clean corer. No snow precipitation was observed throughout the duration of the experiments. Ice samples were melted for a suite of parameters for rows  $T_1$ ,  $T_2$  and  $T_3$ . For  $T_4$ , the core was long enough to cut it into two sections using the Ti-coated handsaw (top = 0.1 m and bottom = the rest of the core). The procedure was achieved under a class-100 laminar flow hood (AirClean 600 PCR workstation, Model 300 Controller, AirClean System).

With the exception of the ice texture sample, ice samples were placed in individual PP melting containers and melted rapidly onboard in the dark at room temperature, according to Rintala et al. (2014). During melting, the sample was gently homogenised to help redistribute the heat evenly and keep the melt cool. Melted ice cores and seawater samples were then immediately processed for particulate organic carbon (POC) and nitrogen (PON), dissolved organic carbon (DOC), the inorganic macro-nutrients ammonium ( $\text{NH}_4^+$ ), silicic acid ( $\text{Si}(\text{OH})_4$ ), phosphate ( $\text{PO}_4^{3-}$ ) and nitrate + nitrite ( $\text{NO}_3^- + \text{NO}_2^- = \text{NO}_3$ ), chlorophyll *a* (Chl *a*), extracellular polymeric substances (EPS), bacterial counts, particulate iron (PFe) and dissolved iron (DFe), and bulk salinity.

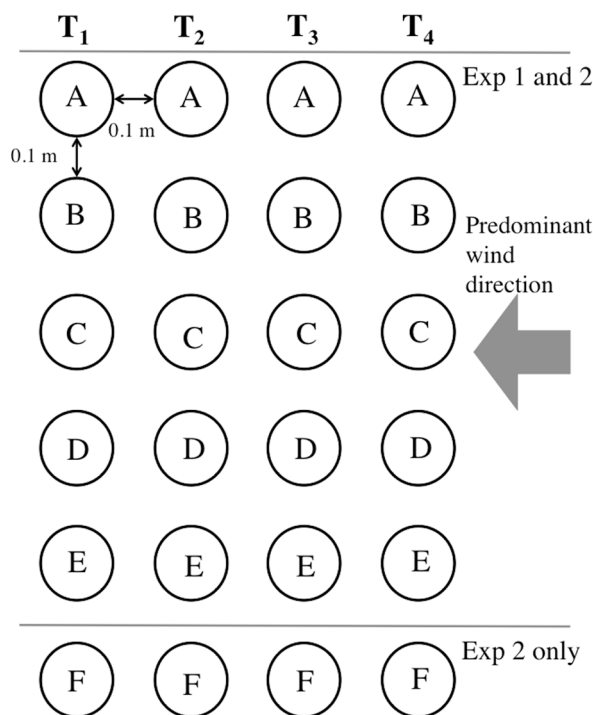


**Figure 2**

Layout of the *in situ* ice-growth experiments.

Layout of the set-up for Exp 1 and 2 (aerial view). Cores were separated by 0.1 m. For each time step, one row (cores A–E for Exp 1 and A–F for Exp 2) was sampled for a suite of parameters.  $T_1$  sampling was at 6 hours,  $T_2$  at 12 hours,  $T_3$  at 24 hours and  $T_4$  at 48 hours. Core allocation was as follows for Exp 1: core A, temperature and ice texture; core B, salinity and bacterial counts; core C, POC/PON, DOC, macro-nutrients and Chl *a*; core D, EPS; and core E, PFe and DFe. Core allocation during Exp 2 was: core A, temperature and ice texture; core B, salinity and bacterial count; core C, POC/PON, DOC, macro-nutrients; core D, Chl *a*; core E, EPS; and core F, PFe and DFe.

doi: 10.12952/journal.elementa.000123.f002

### 2.4 Young natural ice sampling

Seawater was sampled 1 m below the ice using a 5-L polyvinylidene fluoride “PRISTINE” sample bottle (NIOZ) attached to a kevlar hydrographic wire and activated by a Teflon messenger. A subsample was then drawn into LDPE bottles, triple-bagged and brought back to the ship. The methods used to collect natural young ice were adapted to the type of ice (Table 1). Unconsolidated pancake ice was collected from a cage hanging over the sea ice (Station 486). The ice blocks were collected directly by hand, wearing clean-room nitrile gloves and clean sleeves (Kanna et al., 2014). Semi-consolidated pancake ice (Station 488) and consolidated pancake ice (Station 489) were sampled from the cage using the TM-clean corer. Young ice (Station 496) and grey ice (Station 500) were collected upwind from the ship from a refrozen lead.

Grey ice is a type of newly formed sea ice with a thickness of 0.10–0.15 m. It is usually less elastic than nilas (thin sheet of transparent ice) and rafts under pressure. Young ice was collected using a SIPRE-type corer (Kovacs, 9-cm internal diameter). Approximately 1.5 cm of the outer layer of the core was scraped off using a Ti-blade to collect the clean inner core section (Kanna et al., 2014). Grey ice was sampled using the Ti-coated handsaw directly from the ice edge. Only the bottom 0.1 m of the core was analyzed for the semi-consolidated pancake ice, the consolidated pancake and the young ice. Cutting was processed on site to minimize brine loss. The entire core was placed on a trace-metal clean plastic board and cut using a Ti-coated handsaw immediately after sampling. For each station, the collected ice sections were placed in individual TM-clean PP melting containers and brought back to the ship. With the exception of the ice texture sample, samples were allowed to melt onboard in the dark at room temperature (Rintala et al., 2014). The melting time varied from 6 hours to approximately 16 hours for the thicker sections. Seawater and natural sea-ice samples were processed for the same variables as the ice-growth experiments, except for bacterial count, which was determined only for the *in situ* ice-growth experiments.

## 2.5 Analytical techniques

### 2.5.1 Physical variables

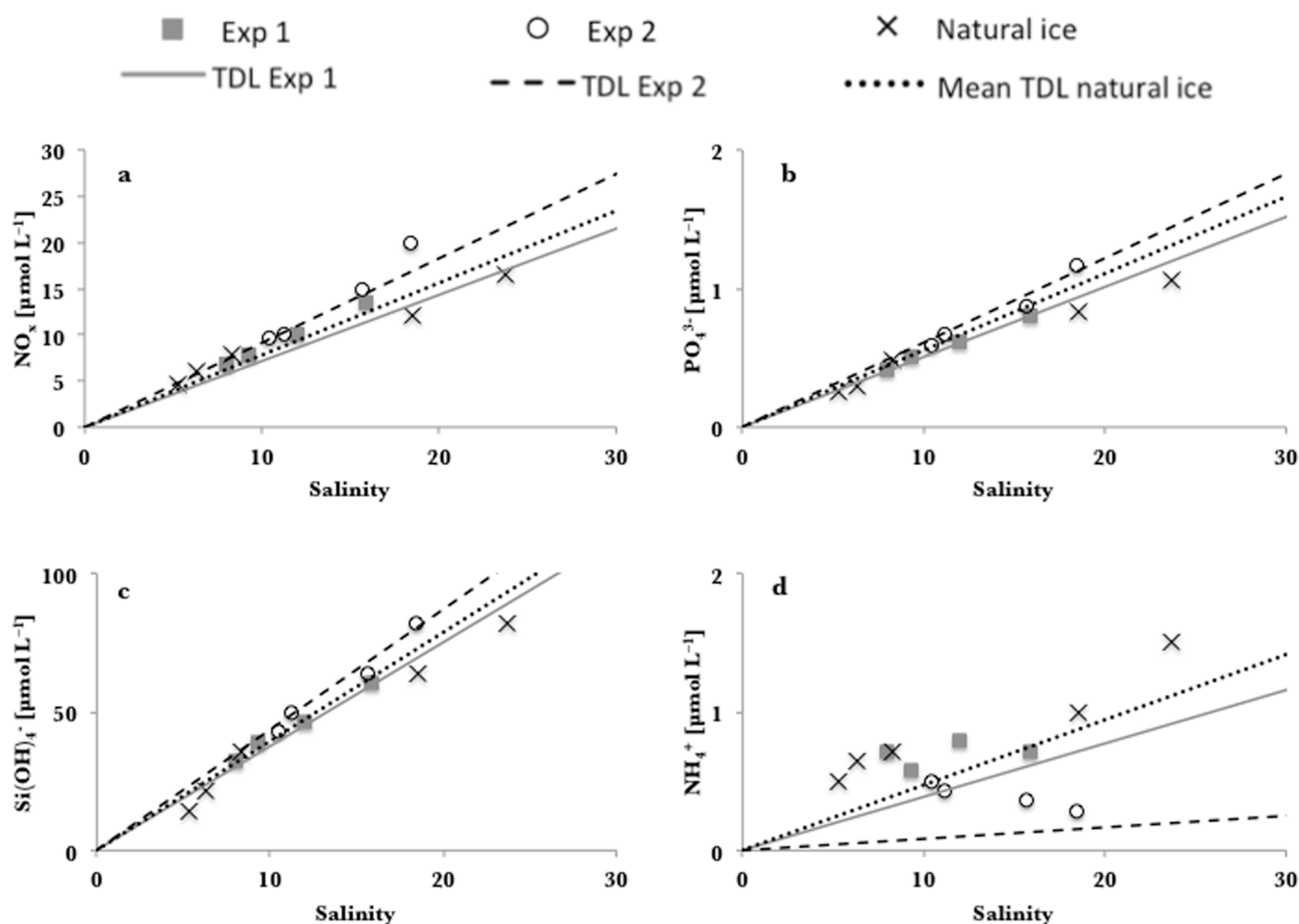
*In situ* ice temperatures were measured using a calibrated probe (Testo 720, precision  $\pm 0.1$  °C) inserted into 4-mm diameter holes freshly drilled into the side (2-cm intervals) of ice core A (Figure 2). Bulk salinity (Practical Salinity,  $S_p$ ) of melted ice samples and seawater samples were measured using an Orion Star 3 conductivity meter (precision  $\pm 0.1$ ). Using the temperature and bulk salinity measurements (core B), brine volume fractions ( $V_b/V$ ) were calculated according to Cox and Weeks (1988), neglecting sea-ice air content. Vertical thin sections of ice cores A were prepared ( $-25$  °C in a ship-board cold room) and analyzed using cross-polarized light to identify ice textures (granular vs. columnar; Langway, 1958).

### 2.5.2 Particulate organic carbon and nitrogen, dissolved organic carbon, and macro-nutrients

All glassware in contact with POC, PON, and DOC samples was combusted at 450°C for 12 hours prior to the cruise. Onboard and immediately after fully melted, ice and seawater samples were gently shaken to homogenize before filtration (200–2,500 mL) onto pre-combusted (450°C, 12 hours) 25-mm quartz filters (Sartorius). Forty-mL subsamples of the filtrate were stored in glass vials at  $-20$ °C in the dark for later DOC analysis. In addition, 20-mL filtrate subsamples were collected in two plastic tubes kept frozen at  $-20$ °C for macro-nutrient analyses. For DOC analyses, frozen samples were melted overnight in the dark, and DOC concentrations were determined by high-temperature catalytic oxidation using a TOC analyzer (Total Organic Carbon Analyzer TOC-L CPH, Shimadzu) following the method of Qian and Mopper (1996). Quality controls were run using a standard of potassium hydrogen phthalate (reagent grade, Nakalai Tesque, Kyoto, Japan) and a solution of hydrogen carbonate and sodium carbonate (reagent grade, Nakalai Tesque, Kyoto, Japan). Detection limit for DOC was 0.33  $\mu\text{mol L}^{-1}$  and precision was 1.5%. Filters for determination of POC/PON were stored at  $-20$ °C until analysis. After drying the filters at 60°C, inorganic carbon was removed by adding 30  $\mu\text{L}$  of 10% (v:v) HCl (Ajax Finichem) to the filters. POC and PON contents on the filter were determined using a Thermo Finnigan EA 1112 Series Flash Elemental Analyzer (detection limit 0.1  $\mu\text{g}$ , precision 1%). Certified standards of sulphanilamide OAS (Elemental Microanalysis Limited, Okehampton, UK) were run every 12 samples to ensure the quality of the POC and PON concentrations. The macro-nutrients  $\text{Si}(\text{OH})_4^-$ ,  $\text{PO}_4^{3-}$ ,  $\text{NH}_4^+$ , and  $\text{NO}_x$  were analyzed at Analytical Service Tasmania following the methods recommended by Grasshoff et al. (1999). Phosphates,  $\text{NH}_4^+$  and  $\text{NO}_x$  were analyzed with a Lachat Flow injection analyser (precision 0.5%). The detection limit is 0.002  $\text{mg L}^{-1}$  for each parameter. Silicic acid was analyzed using a photometric analyzer (Aquamem 250) with a detection limit of 0.1  $\text{mg L}^{-1}$  and precision of 2%. Measured certified reference material for nutrients in seawater (RMNS, Kanso, Japan) were run to ensure the quality of the nutrient concentrations. Theoretical dilution lines (TDL; Figure 3) were calculated using the macro-nutrient concentration of the underlying seawater sampled at the beginning of each experiment (Meese, 1989).

### 2.5.3 Iron

All onboard manipulations for Fe determinations were conducted under a class-100 laminar flow hood (AirClean 600 PCR workstation, Model 300 Controller, AirClean System). Sea-ice samples were allowed to melt in acid-clean PP buckets at room temperature in the dark. Immediately after melting, dissolved Fe ( $\text{DFe} < 0.4 \mu\text{m}$ ) was obtained by collecting 60 mL of the filtrate passed through a 0.4- $\mu\text{m}$  pore size 47-mm diameter polycarbonate (PC) membrane filter (Sterlitech) using a Teflon perfluoroalkoxy (PFA) filtration apparatus (Saville, USA) under gentle vacuum ( $< 0.13$  bar) to avoid cell lysis. Polycarbonate filters retaining the particulate Fe fraction ( $\text{PFe} > 0.4 \mu\text{m}$ ) were transferred into acid-clean petri-dishes, double-bagged and stored at  $-20$ °C in the dark until analysis after return to Australia. DFe samples were collected in LDPE bottles (Nalgene) and acidified to pH 1.8 using 12 M ultra pure hydrochloric acid (Seastar Baseline, Choice Analytical). Samples were stored double-bagged at room temperature for at least 24 hours before measurement by flow injection analysis with chemiluminescent detection (FIA-CL).



**2.5.3.1 Dissolved Fe.** DFe samples were analyzed using a FIA-CL instrument. FIA-CL followed procedures by Obata et al. (1993) and de Jong et al. (1998), as described in detail by van der Merwe et al. (2009). The detection limit of the FIA-CL method is calculated as three times the standard deviation (SD) of the procedural blank. Quality controls were run using international seawater reference samples (Sampling and Analysis of Fe (SAFe), deep (D2) and shallow (S), with consensus values of  $0.960 \pm 0.024 \text{ nmol L}^{-1}$  and  $0.096 \pm 0.082 \text{ nmol L}^{-1}$ ,  $n = 4$ , respectively).

**2.5.3.2 Particulate Fe.** PFe polycarbonate filters were digested in 15 mL Teflon PFA vials (Savillex, USA), heated at  $95^\circ\text{C}$  for 12 hours on a Teflon coated hotplate (SCP Science), within an ISO 5 ducted laminar flow bench, housed within an ISO 7 clean room, using a mixture of 250  $\mu\text{L}$  HCl (12 M, Seastar Baseline, Choice Analytical), 250  $\mu\text{L}$  HNO<sub>3</sub> (16 M, Seastar Baseline, Choice Analytical) and 500  $\mu\text{L}$  HF (29 M, Seastar Baseline, Choice Analytical). The PFA vials were allowed to cool down before being dry evaporated for 4 hours at  $60^\circ\text{C}$ . The samples were then re-suspended in 10 mL ultrapure 2% (v:v) HNO<sub>3</sub> with addition of indium as an internal standard to a final concentration of 10 ppb. Concentrations of PFe were determined at the Central Science Laboratory (University of Tasmania) using an Inductively Coupled Plasma Mass Spectrometer (ICP-MS, Element 2) according to Bowie et al. (2010). Prior to analysis, the instrument was purged with alternate 5% (v:v) HCl and 5% (v:v) HNO<sub>3</sub> solutions for 1 hour. Finally a 2% (v:v) HNO<sub>3</sub> solution was used to condition the instrument. A linear calibration curve was created using solutions of 0, 1, 5 and 10 ppb of a mixed standard (QCD Analysts, MISA suite of solutions, Spring Lake, USA). Samples were handled in a class-100 laminar flow bench. To ensure a low background recovery the instrument was rinsed with a solution of 2% (v:v) HNO<sub>3</sub>, and a calibration blank (0 ppb) was analyzed as an unknown ( $n = 3$ ). A 10 ppb mixed standard used to monitor instrument drift showed good instrument stability during analysis. Analyses of a certified reference material (BCR-414) resulted in a measured mean Fe value ( $\pm$  SD,  $n = 3$ ) of  $1.76 \pm 0.04 \text{ g kg}^{-1}$  compared to the certified (indicative) value of  $1.85 \text{ g kg}^{-1}$ , for a recovery of  $95.2 \pm 2.07\%$ . The mean value for procedural digested acid blanks ( $n = 3$ ) was  $0.146 \pm 0.028 \text{ } \mu\text{g Fe L}^{-1}$ ; the mean value for filter blanks ( $n = 3$ ) was  $3.255 \pm 0.829 \text{ } \mu\text{g Fe L}^{-1}$ . The limit of detection was calculated as three times the standard deviation of the blank, which was  $0.085 \text{ } \mu\text{g Fe L}^{-1}$  for the acid blank and  $2.488 \text{ } \mu\text{g Fe L}^{-1}$  for the filter blank.

**Figure 3**  
Concentrations of macro-nutrients and their theoretical dilution lines.

Concentration ( $\mu\text{mol L}^{-1}$ ) of a) nitrate + nitrite ( $\text{NO}_x$ ), b) phosphate ( $\text{PO}_4^{3-}$ ), c) silicic acid ( $\text{Si(OH)}_4$ ) and d) ammonium ( $\text{NH}_4^+$ ) plotted against salinity for Exp 1 and 2 and the natural young ice. The solid grey line represents the theoretical dilution line (TDL) for Exp 1, the dashed dark line represents the TDL for Exp 2 and the dotted dark line represents the mean TDL for the natural young ice samples ( $n = 5$ ). The TDLs are based on the salinity and respective macro-nutrient concentrations in underlying seawater.

doi: 10.12952/journal.elementa.000123.f003

### 2.5.4 Extracellular polymeric substances

Melted ice and seawater samples were homogenized and filtered in triplicate onto 25-mm 0.4- $\mu\text{m}$  pore size PC membranes (Millipore) under low vacuum ( $< 0.13$  bar). A volume of 500  $\mu\text{L}$  of 0.2- $\mu\text{m}$  pre-filtered 0.02% Alcian Blue (AB, GX8 Sigma) in 0.06% acetic acid was added directly onto the filter and drawn through at low vacuum. If the AB stayed on the sample for more than 2 seconds, the filter was considered clogged and discarded. The filters were rinsed with 2 mL of Milli-Q water (Millipore, Gradient A10) to remove excess dye, placed in a PCR-well and stored in the dark at  $-20^\circ\text{C}$  until further analysis. A calibration curve was performed at the start and the end of the cruise. The calibration curve was achieved by filtering 0, 5, 10 and 12 mL of a stock solution of 100  $\text{mg L}^{-1}$  of xanthan gum (Sigma-Aldrich). One filter blank was collected on every sampling day. EPS concentrations were determined using the colorimetric AB method (Passow and Alldredge, 1995) modified by van der Merwe et al. (2009). The semi-quantitative AB method is based on the affinity of the AB stain for acid polysaccharides. The method targets particles  $> 0.4 \mu\text{m}$  and does not penetrate cells. Briefly, samples were extracted in 3 mL of 80% (v:v) sulphuric acid ( $\text{H}_2\text{SO}_4$ ) (reagent grade, Merck Germany), measured spectrophotometrically with a Halo RB-10 spectrophotometer, and expressed in units of xanthan gum equivalents (xeq). The standard deviation between triplicates was  $< 10\%$ .

### 2.5.5 Chlorophyll *a* and bacterial counts

Ice cores were melted rapidly, with gentle shaking, at room temperature in the dark for Chl *a* analysis (Rintala et al., 2014). Melted samples were filtered under low vacuum ( $< 0.13$  bar) and low light immediately after melting. To distinguish the contribution of larger autotrophs ( $\mu\text{Chl } a > 10 \mu\text{m}$ ) and smaller autotrophs ( $10 \mu\text{m} > \mu\text{Chl } a > 0.8 \mu\text{m}$ ), samples were size-fractionated by sequentially filtering the sample first onto 10- $\mu\text{m}$  and then 0.8- $\mu\text{m}$  polycarbonate filters (Millipore, 47-mm diameter). Filters were extracted in acetone and measured fluorometrically using a Turner Designs 10AU fluorometer (in vitro detection limit 0.02  $\mu\text{g L}^{-1}$ ) according to Arar and Collins (1997). Volumes of 20 mL of sea ice and seawater samples from the two *in situ* experiments were fixed with glutaraldehyde (microscopy grade, final concentration of 1%) for bacterial counting. Samples were stored at  $4^\circ\text{C}$  until analysis at the Finnish Environmental Institute. They were then stained with Acridine Orange and counted by epifluorescence microscopy using a Leitz Aristoplan epifluorescence microscope equipped with I3 filter and PL Fluotar 100 x 12.5/20 oil immersion objective.

## 2.6. Cross-variable statistics

To evaluate the relationships between variables, non-parametric Spearman's rank correlations were used. For  $p < 0.05$ , the strength of the relationship was determined according to Cohen (1988). Data from *in situ* growth experiments and natural young ice samples were pooled together for analysis.

## 2.7 Enrichment index

For each parameter we calculated the enrichment index,  $EI_x$  (Gradinger and Ikävalko, 1998). This index is based on the effective segregation coefficient  $k_{\text{eff},x}$  of the component  $x$  and is normalized to salinity to detect specific incorporation processes that differ from conservative behavior with bulk salinity.

$$EI_x = \frac{[\text{Sal}]_{\text{source}}}{[\text{Sal}]_{\text{ice}}} \cdot \frac{[\text{X}]_{\text{ice}}}{[\text{X}]_{\text{source}}} \quad (1)$$

where  $[\text{Sal}]_{\text{source}}$  and  $[\text{Sal}]_{\text{ice}}$  are the salinity of the underlying seawater and the bulk salinity of the ice, respectively,  $[\text{X}]_{\text{ice}}$  is the concentration of the component in the ice and  $[\text{X}]_{\text{source}}$  is the concentration of the component  $x$  in the underlying seawater. Values of 1,  $< 1$  or  $> 1$  will correspond to conservative, specifically depleted or specifically enriched as compared to bulk salinity, respectively.

# 3. Results

## 3.1 *In situ* ice-growth time-series experiments

### 3.1.1 Basic sea-ice properties

Experiment 1 (Exp 1) was carried out on a first-year sea-ice floe in the central Weddell Sea (Station 506, Figure 1). Ice thickness and snow thickness ranged between 0.45 m and 0.71 m (average  $\pm$  SD:  $0.58 \pm 0.09$  m,  $n = 15$ ), and between 0.12 m and 0.17 m (average  $\pm$  SD:  $0.145 \pm 0.018$  m,  $n = 10$ ), respectively.

Experiment 2 (Exp 2) was located in the western part of the Weddell Sea (Station 517, Figure 1), closer to the continental shelf. The site had a more rafted and ridged ice cover, and a thicker snow cover (average  $\pm$  SD:  $0.34 \pm 0.02$  m,  $n = 10$ ).

During the experiments, total ice thickness after 48 hours reached 0.24 m in Exp 1 and 0.22 m in Exp 2. The ice thickness and ice-growth rate at the end of each time step are summarized in Table 2.

Table 2. Physical properties of the *in situ* ice-growth time-series samples from experiments 1 and 2

Sampling time		Ice thickness (m)		Growth rate (cm h <sup>-1</sup> )		Temperature (°C)		Bulk salinity (S <sub>p</sub> )		V <sub>b</sub> /V (%) <sup>a</sup>	
Designation	Time step (h)	Exp 1	Exp 2	Exp 1	Exp 2	Exp 1	Exp 2	Exp 1	Exp 2	Exp 1	Exp 2
T <sub>1</sub>	0–6	0.030	0.045	0.50	0.75	-4.2	-5.2	15.9	18.4	18	17
T <sub>2</sub>	0–12	0.065	0.060	0.54	0.50	-4.2	-5.9	12.0	15.7	14	13
T <sub>3</sub>	0–24	0.085	0.095	0.35	0.40	-4.0	-6.9	9.3	11.2	12	9
T <sub>4</sub>	0–48	0.240	0.225	0.50	0.40	-6.7	-9.9	8.0	10.4	7	6

<sup>a</sup> V<sub>b</sub>/V = Brine volume fraction  
doi: 10.12952/journal.elementa.000123.r002

We observed a thin layer of granular ice at the surface of the newly formed sea ice (0.030 m in Exp 1 and 0.025 m in Exp 2) followed by columnar ice in both experiments. Columnar ice started to grow after 6 hours in Exp 1 and less than 6 hours in Exp 2, reflecting the pattern of natural ice formation (Figure S1a, b). Given the geometry of the experimental set up, however, it is worth noting that as the new columnar ice started to grow, progressive insulation from the ice at the top introduced competition with lateral growth from the cold sides of the initial core hole (surrounding ice floe); the effect actually dominated from a depth comparable to the diameter of the initial hole. The bulk ice salinity decreased from T<sub>1</sub> to T<sub>4</sub> as expected for growing sea ice (Table 2). Ice temperatures were slightly lower during Exp 2 driven by colder air temperatures (Table 2). Average air temperature was  $-18.3 \pm 2.0^\circ\text{C}$  (n = 297) during Exp 1 and  $-24.8 \pm 2.7^\circ\text{C}$  during Exp 2 (n = 294). Despite the low ice temperatures, brine volumes (V<sub>b</sub>/V) were all above the 5% theoretical percolation threshold for columnar ice, indicating a high porosity and therefore permeable nature of the newly formed ice (Golden et al., 1998). Note that V<sub>b</sub>/V, temperature and salinity values were averaged for the entire core in T<sub>4</sub> (n = 2). Mean  $\pm$  SD reported for the results described below (3.1.2–3.1.4) refer to one value per time step (n = 4).

### 3.1.2 Macro-nutrients, particulate organic carbon and nitrogen, and dissolved organic carbon

Nitrate + nitrite (NO<sub>x</sub>), PO<sub>4</sub><sup>3-</sup> and Si(OH)<sub>4</sub><sup>-</sup> showed similar temporal trends in both experiments (data not shown). The highest macro-nutrient concentrations were found in the T<sub>1</sub> cores, while the lowest concentrations were found in the T<sub>4</sub> cores. When plotted against salinity, NO<sub>x</sub>, PO<sub>4</sub><sup>3-</sup> and Si(OH)<sub>4</sub><sup>-</sup> followed theoretical dilution lines (TDL) (Figure 3 a–c). Ammonium concentrations in sea ice behaved differently compared to the other macro-nutrients, deviating from the TDL (Figure 3d). Concentrations above the TDL suggest that different processes are involved in the incorporation or production of NH<sub>4</sub><sup>+</sup>, leading to the enrichment of NH<sub>4</sub><sup>+</sup> in the ice.

Unlike macro-nutrients, POC was enriched in sea ice compared to underlying seawater. In general, POC and PON exhibited a bell-shaped temporal development in both experiments. POC concentrations in the ice in Exp 1 and 2 ranged from 2.9 to 13.6  $\mu\text{mol L}^{-1}$  and from 8.5 to 15.0  $\mu\text{mol L}^{-1}$ , respectively (Figure S2a, b). The underlying seawater concentrations were an order of magnitude lower, with 1.5  $\mu\text{mol L}^{-1}$  and 0.5  $\mu\text{mol L}^{-1}$  for Exp 1 and 2, respectively. In both experiments, PON concentrations were higher than the underlying seawater concentrations. Molar POC:PON ratios in the underlying seawater were below the typical Redfield ratio of 6.6 for phytoplankton, while ratios were consistently higher in the ice, with mean values of  $12.5 \pm 5.1$  and  $11.7 \pm 2.1$  for Exp 1 and 2, respectively. DOC concentrations were below the detection limit of 0.33  $\mu\text{mol L}^{-1}$  in underlying seawater and sea ice in both experiments.

### 3.1.3 EPS, Chl *a* and bacterial counts

Even when filtering for EPS at low pressure (< 0.13 bar) using the AB method, only a fraction of the material is retained on the filter (Passow and Alldredge, 1995). We computed EPS concentrations using a filter-capture efficiency for xanthan gum of 4.4% (van der Merwe et al., 2009). Although the EPS concentrations were higher in Exp 2 than in Exp 1, their evolution as a function of time was similar and displayed a bell-shaped development. Concentrations in the ice varied from 0.17 to 0.66  $\mu\text{g xeq L}^{-1}$  (average:  $0.38 \pm 0.21 \mu\text{g xeq L}^{-1}$ ) in Exp 1. In Exp 2, the concentrations ranged from 0.54 to 0.98  $\mu\text{g xeq L}^{-1}$  (average:  $0.75 \pm 0.23 \mu\text{g xeq L}^{-1}$ ). Concentrations in the underlying seawater were 0.22  $\mu\text{g xeq L}^{-1}$  and 0.66  $\mu\text{g xeq L}^{-1}$  for Exp 1 and 2, respectively (Figure S3a, b).

The total Chl *a* (TotChl *a* = iChl *a* + sChl *a*) concentration in sea ice showed large variations with a peak at T<sub>3</sub> in Exp<sub>1</sub> (Figure S3a). No corresponding peak was observed in Exp 2 (Figure S3b). Concentrations in sea ice varied between 0.04 and 0.52  $\mu\text{g L}^{-1}$  in Exp 1, and 0.03 and 0.17  $\mu\text{g L}^{-1}$  in Exp 2 (Figure S3b). TotChl *a* concentrations in underlying seawater were low: below the detection limit for Exp 1, and 0.02  $\mu\text{g L}^{-1}$  for Exp 2 (Figure S3a, b). Large autotrophs were virtually absent in the water but often made up the largest fraction in the ice, representing 57–92% (average:  $78 \pm 15\%$ ) of the TotChl *a* concentration in Exp 1 and 22–57% (average:  $39 \pm 15\%$ ) in Exp 2.

Bacterial concentrations in the ice varied between  $1.15 \times 10^5$  and  $2.90 \times 10^5$  cells  $\text{mL}^{-1}$  in Exp 1 and between  $9.53 \times 10^4$  and  $2.22 \times 10^5$  cells  $\text{mL}^{-1}$  in Exp 2. The temporal evolution of bacterial numbers in the ice was similar in both experiments with highest concentrations found at  $T_1$  and the lowest at  $T_4$ . Bacterial concentrations in underlying seawater were  $2.95 \times 10^5$  cells  $\text{mL}^{-1}$  for Exp 1 and  $1.96 \times 10^5$  cells  $\text{mL}^{-1}$  for Exp 2 (Figure S4).

### 3.1.4 Iron

Similar to the other particulate fractions, PFe was enriched in sea ice compared to underlying seawater. Particulate Fe concentrations ranged from 7.8 to 55.5  $\text{nmol L}^{-1}$  in Exp 1 and 10.1 to 62.5  $\text{nmol L}^{-1}$  in Exp 2 (Figure S5a, b). Average concentrations were similar in both experiments (Exp 1:  $23.7 \pm 21.5$   $\text{nmol L}^{-1}$ ; Exp 2:  $26.1 \pm 24.4$   $\text{nmol L}^{-1}$ ). Underlying seawater values were 4.5  $\text{nmol L}^{-1}$  in Exp 1 and 1.6  $\text{nmol L}^{-1}$  in Exp 2. The highest values were observed at  $T_2$  in both experiments. Dissolved Fe was also enriched in sea ice compared to seawater and the temporal evolution of DFe concentrations was similar in both experiments (Figure S5a, b). Average DFe concentrations in Exp 1 and 2 were  $1.0 \pm 0.2$   $\text{nmol L}^{-1}$  and  $1.7 \pm 1.3$   $\text{nmol L}^{-1}$ , respectively. PFe:DFe ratios behaved similarly. All ratios in the ice were higher ( $22.4 \pm 16.9$  in Exp 1 and  $16.5 \pm 7.2$  in Exp 2) than the underlying seawater ratios (7.0 in Exp 1 and 4.7 in Exp 2).

## 3.2 Natural young ice

In this section, when discussing seawater concentrations and TDLs we refer to the average seawater concentration ( $n = 5$ ) using under-ice seawater data from the five sampling sites where natural young sea ice was collected, unless mentioned otherwise.

### 3.2.1 Basic sea-ice properties

The ice samples collected at stations 486, 488 and 489 represented different stages of pancake ice formation (Table 1). The first stage sampled (Station 486) was a large, thin and unconsolidated pancake with a thickness of 0.06–0.07 m. The second stage was a semi-consolidated pancake (Station 488) of 0.30–0.36 m in thickness. Snow was absent on the unconsolidated pancake and less than 0.01 m thick on the semi-consolidated pancake. At station 489, the snow cover was 0.03 m and the ice 0.30–0.36 m thick. Here pancakes were highly consolidated. Thin ice was also collected at station 496 with a 0.45 m average thickness and covered with 0.04 m of snow (Table 1). The grey ice (Station 500) was 24 hours old and 0.05–0.07 m thick (Table 1).

Elongated crystals of granular ice were observed in the unconsolidated pancake. Ice textures of the semi-consolidated and consolidated pancake exhibited classic patterns of granular ice underlain with columnar ice. We observed an intrusion of granular ice between 0.23 and 0.26 m in the consolidated pancake, suggesting rafting events (Figure S6c). The bottom of the thin ice core (Station 496) was columnar (data not shown) and the grey ice sample (Station 500) was too soft to process for ice texture analysis.

Bulk ice salinities of natural ice samples ranged from 5.3 (semi-consolidated pancake) to 23.7 (unconsolidated pancake) with an average of  $12.4 \pm 8.2$  ( $n = 5$ ). Computed brine volumes of natural ice samples ranged from 6.2 to 28.0% (average:  $16.5 \pm 9.9\%$ ,  $n = 5$ ; Table 1).

### 3.2.2 Macro-nutrients, particulate organic matter and dissolved organic carbon

Macro-nutrient concentrations in natural young ice were lower than in the underlying seawater, except for  $\text{NH}_4^+$  in the unconsolidated pancake. Ammonium ranged from 0.50  $\mu\text{mol L}^{-1}$  to 1.50  $\mu\text{mol L}^{-1}$ ;  $\text{NO}_x$ , from 4.71  $\mu\text{mol L}^{-1}$  to 16.4  $\mu\text{mol L}^{-1}$ ;  $\text{PO}_4^{3-}$ , from 0.26  $\mu\text{mol L}^{-1}$  to 1.06  $\mu\text{mol L}^{-1}$ ; and  $\text{Si(OH)}_4^-$ , from 14.2  $\mu\text{mol L}^{-1}$  to 81.9  $\mu\text{mol L}^{-1}$ . Similar to Exp 1 and 2, all macro-nutrients followed TDLs, except for  $\text{NH}_4^+$  which showed elevated concentrations in sea ice compared to background seawater levels (Figure 3). POC and PON concentrations were one order of magnitude higher in sea ice than in the underlying seawater (Figure S2c). Average underlying seawater concentrations for POC and PON were  $2.1 \pm 1.3$   $\mu\text{mol L}^{-1}$  and  $0.24 \pm 0.05$   $\mu\text{mol L}^{-1}$ , respectively. Molar POC:PON ratios were of the same order of magnitude in the ice and the underlying seawater and higher than the Redfield ratio in all collected natural ice samples (Figure S2c). DOC values were below the detection limit of 0.33  $\mu\text{mol L}^{-1}$  for all natural ice and underlying seawater samples, except in two ice bottom sections (data not shown).

### 3.2.3 Biological data: EPS and Chl *a*

The average EPS concentration in underlying seawater was  $0.62 \pm 0.30$   $\mu\text{g xeq L}^{-1}$  (Figure S3c). Except for the bottom part of the consolidated pancake ice, EPS concentrations were higher in the underlying seawater than in the young ice for each station. The highest concentration in the ice was observed in the grey ice sample ( $0.86$   $\mu\text{g xeq L}^{-1}$ ) and the lowest in the unconsolidated pancake ( $0.11$   $\mu\text{g xeq L}^{-1}$ ; Figure S3c).

Similar to POC, PON and EPS, salinity-normalized Chl *a* in sea ice was enriched in comparison to underlying seawater (Figure S3c). The bottom section of the consolidated pancake ice displayed the highest *TotChl a* concentration ( $2.2$   $\mu\text{g L}^{-1}$ ) while the lowest concentration was detected in the grey ice ( $< 0.1$   $\mu\text{g L}^{-1}$ ). Compared to the small autotrophs, large autotrophs were more enriched in the young ice. *iChl a* contributed up to 86% (average:  $70 \pm 15\%$ ,  $n = 5$ ) of the *TotChl a* in the natural young ice.

### 3.2.4 Iron

Because of possible contamination occurring during sampling, the Fe data for the unconsolidated pancake and associated seawater sample (254 nmol L<sup>-1</sup> and 52.8 nmol L<sup>-1</sup> of PFe, respectively) were discarded from the dataset. The dissolved Fe concentration in the seawater at this sampling site was 1.9 nmol L<sup>-1</sup>, while there was no sea-ice DFe data available for this station.

For all other stations, PFe was enriched in sea ice with concentrations ranging from 20.1 to 76.7 nmol L<sup>-1</sup> (average: 40.4 ± 25.0 nmol L<sup>-1</sup>, n = 4) compared to 0.3 to 0.9 nmol L<sup>-1</sup> (average: 0.6 ± 0.4 nmol L<sup>-1</sup>, n = 4) in the underlying seawater (Figure S5c). Dissolved Fe was also enriched in natural sea ice compared to its underlying seawater. DFe concentrations in the ice ranged from 1.0 nmol L<sup>-1</sup> in the semi-consolidated pancake to 3.2 nmol L<sup>-1</sup> in grey ice. The average sea-ice DFe concentration was 1.8 ± 1.0 nmol L<sup>-1</sup> (n = 4). Underlying seawater concentrations ranged from 0.2 nmol L<sup>-1</sup> to 0.4 nmol L<sup>-1</sup> (average of 0.3 ± 0.1 nmol L<sup>-1</sup> (n = 4), Figure S5c). For both PFe and DFe, the highest concentration was detected in the grey ice sample. The average PFe and DFe concentrations in natural young ice were of the same order of magnitude as in Exp 1 and 2. Similar to our observations in Exp 1 and 2, PFe:DFe ratios in the ice were elevated relative to the ratio in the underlying seawater (Figure S5c). The average ratio (22.5 ± 9.0, n = 4) in young ice was comparable to the experimental average.

### 3.3 Property–property relationships

Using the combined dataset from both experiments and natural ice samples, significant correlations (Spearman's rho, p < 0.05) were observed for PFe and DFe (rho = 0.829, n = 14) and bacteria and brine volume (rho = 0.830, n = 10) for *in situ* samples and natural samples. There were strong inverse correlations between EPS and NH<sub>4</sub><sup>+</sup> (rho = -0.828, n = 15), and POC and brine volume (rho = -0.593, n = 15). Temperature was strongly inversely correlated with macro-nutrients except for NH<sub>4</sub><sup>+</sup>. Bacteria, *TotChl a* and EPS were positively correlated with temperature (rho = 0.733, n = 10; rho = 0.529, n = 15; and rho = 0.518, n = 15, respectively). No correlations were observed between EPS and *TotChl a*, EPS and DFe, and EPS and PFe.

### 3.4 Enrichment indices

The enrichment indices for Exp 1 and 2 and natural young ice are summarized in Table 3. Because the *Chl a* concentrations in seawater in Exp 1 were below the detection limit, enrichment indices for *Chl a* in

**Table 3. Enrichment indices<sup>a</sup> for biogeochemical parameters of *in situ* ice-growth time-series<sup>b</sup> experiments and natural young ice samples**

Parameter	Experiment 1				Experiment 2				Natural young ice <sup>c</sup>
	T <sub>1</sub>	T <sub>2</sub>	T <sub>3</sub>	T <sub>4</sub>	T <sub>1</sub>	T <sub>2</sub>	T <sub>3</sub>	T <sub>4</sub>	
NH <sub>4</sub> <sup>+</sup>	1.2	1.7	1.6	2.3	1.9	2.7	4.6	6.0	1.80±0.80
NO <sub>x</sub>	1.2	1.2	1.2	1.2	1.2	1.0	1.0	1.1	1.1±0.20
PO <sub>4</sub> <sup>3-</sup>	1.0	1.0	1.1	1.0	1.0	0.9	1.0	1.0	0.9±0.1
Si(OH) <sub>4</sub> <sup>-</sup>	1.0	1.0	1.1	1.1	1.0	0.9	1.0	1.0	0.9±0.1
POC	0.3	3.2	3.3	4.3	51	65	52	95	61±49
PON	7.3	7.6	6.8	13	7.4	7.9	9.6	17	36.2±36.6
EPS	7.5	4.2	3.3	9.7	2.8	3.0	2.5	3.0	3.2±3.0
<i>lChl a</i> <sup>d</sup>	ND <sup>e</sup>	ND	ND	ND	52	220	80	150	190±190
<i>sChl a</i> <sup>e</sup>	ND	ND	ND	ND	18	16	16	20	50±125
<i>TotChl a</i> <sup>f</sup>	ND	ND	ND	ND	21	34	22	35	120±120
Bacteria	2.4	1.4	3.4	1.9	2.1	1.4	2.8	1.7	ND
PFe	7.7	40	7.3	19	20	88	30	22	301±240
DFe	4.3	6.1	6.1	6.0	6.9	23	16	4.1	24±10

<sup>a</sup>Values of 1, < 1 or > 1 correspond to conservative, specifically depleted or specifically enriched, respectively, relative to bulk salinity.

<sup>b</sup>Sampling times, T<sub>1</sub>–T<sub>4</sub>, were at 6, 12, 24, and 48 hours.

<sup>c</sup>Average ± SD is provided for the natural young ice samples, where n = 5 for macro-nutrients, POC, PON, EPS, *lChl a*, *sChl a*, *TotChl a*; n = 4 for PFe and DFe.

<sup>d</sup>*lChl a* refers to *Chl a* > 10 μm.

<sup>e</sup>*sChl a* refers to 10 μm > *Chl a* > 0.8 μm.

<sup>f</sup>*TotChl a* refers to *lChl a* + *sChl a*.

<sup>g</sup>ND = No data; seawater values were below detection limit for *Chl a* and not available for bacteria.

doi: 10.12952/journal.elementa.000123.t003

this experiment were not calculated. Enrichment indices for natural samples were calculated using the corresponding seawater concentrations.

The enrichment indices confirmed the conservative behavior of all macro-nutrients, except  $\text{NH}_4^+$ . Enrichment indices for all other variables were higher, with values ranging from 1.4 to greater than 200 confirming a non-conservative behavior relative to salinity. In Exp 2, *l*Chl *a* showed the highest overall enrichment index (average:  $125 \pm 74.2$ ,  $n = 4$ ). Particulate Fe was most enriched in the natural young ice with an average EI of  $301 \pm 240$  ( $n = 4$ ).

## 4. Discussion

Our *in situ* ice-growth experiments provide a new approach to study the incorporation of Fe and organic matter into sea ice. Each experiment can be interpreted as a time-series mimicking the onset of sea-ice formation. In addition to these experiments, we collected natural young ice at several locations. The thickest natural ice sample was 0.45 m thick. Therefore, we believe that our natural samples are only hours or a few days old, as sea ice thermodynamically can only grow up to 0.1 m in a single day (Petrich and Eicken, 2010).

### 4.1 Sea-ice physical properties during experimental and natural conditions

The development of granular ice at the sea-ice surface during the onset of sea-ice formation followed by columnar ice growth, e.g., as observed during Exp 1 and 2, is typical for natural sea-ice growth under calm conditions (Petrich and Eicken, 2010). Ice crystal orientation at  $T_4$  suggests that some ‘side-freezing’, due to heat exchange with the surrounding ice floes, occurred in our experiments after 24 h. This effect was also observed in the bottom section of the  $T_3$  core in Exp 1 (Figure S1a). As discussed further in section 4.3.1, ‘side-freezing’ may have affected initial incorporation of material and brine dynamics in the bottom part of the cores.

Columnar ice formation is generally slower than granular ice formation through frazil accretion (Petrich and Eicken, 2010), and thus impurities are rejected more efficiently (Palmisano and Garrison, 1993; Weissenberger and Grossmann, 1998; Weeks, 2010). In accordance with these previous studies, ice bulk salinities were higher for the first experimental time steps when granular ice was the dominating ice type.

The lower air temperatures during Exp 2 resulted in a faster ice-growth rate during the first 6 hours of the experiment. Despite the cold air temperatures, the ice was relatively warm in both experiments. Indeed ice surface temperatures generally decrease slowly after the initial stage of formation (e.g., Notz and Worster, 2008). Under these conditions, the ice is permeable and gravity drainage possibly occurs within the ice cover.

The irregular size and shape of ice crystals observed in the unconsolidated pancake resembled the texture of the first stages of pancake ice formation (Lange et al., 1989; Figure S6a). Conditions at station 486 were very dynamic physically, which may explain the differences in this sample compared to other ice samples collected under calmer conditions further from the ice edge. These differences are revealed by the ratio between granular and columnar ice in the natural samples decreasing with increasing distance from the ice edge: granular ice represented 83% of the total ice in the unconsolidated pancake and 53% in the consolidated pancake. Brine volumes ( $V_v/V$ ) were always higher than the 5% percolation threshold for columnar ice (Golden et al., 1998) indicating the permeable nature of the ice in all samples.

### 4.2 Incorporation of dissolved constituents: Conservative and non-conservative behavior

Macro-nutrient concentrations in sea ice are controlled by both physical and biological processes, including convective exchanges, nutrient assimilation and assimilation and remineralization by organisms. Both high macro-nutrient concentrations and no deviation from the TDL exclude biological incorporation/accumulation processes in our study. Macro-nutrient EI values close or equal to 1 indicate that the incorporation of macro-nutrients was coupled with sea salt dynamics (i.e., conservative behavior), except for  $\text{NH}_4^+$  (Table 3). Conservative behavior of macro-nutrients has been observed previously in young sea ice (e.g., Dieckmann et al., 1991), which suggests that the processes involved in our ice-growth experiments were similar to those occurring in “naturally” forming ice. Although N, Si and P behaved conservatively with salinity,  $\text{NH}_4^+$  was generally enriched relative to salts. This observation is in line with findings from previous studies (Becquevort et al., 2009; Zhou et al., 2013). The causes for  $\text{NH}_4^+$  enrichment remain unclear, but it has been suggested that, due to its molecular size and shape,  $\text{NH}_4^+$  could become incorporated into the ice crystal structure and not rejected into the brine system like other macro-nutrients (Gross, 2003).

It has been suggested that the seasonal stages of sea-ice formation control the stocks of DFe in sea ice (Lannuzel et al., 2010). Although our DFe concentrations are relatively low compared to other studies collected in winter, spring and summer (Westerlund and Öhman, 1991; de Jong et al., 1998; Lannuzel et al., 2007, 2008, 2013, 2014a; van der Merwe et al., 2009, 2011a), our study provides the first evidence that sea ice begins to accumulate DFe as soon as it forms and grows in late autumn and early winter. Following this initial physico-chemical enrichment, DFe concentrations in sea ice subsequently increase as the ice ages through

the season, likely due to biogenic processes (Lizotte, 2003; Thomas et al., 2010) or detrital remineralization processes, e.g., transformation of PFe into DFe.

Ammonium and DFe were the only two dissolved components in our study showing a non-conservative behavior by enrichment in the ice. Lannuzel et al. (2015) suggested that negatively charged dissolved EPS would complex DFe and, aided by their stickiness, lead to the enrichment of DFe in sea ice. Similar processes have been suggested for  $\text{NH}_4^+$  (e.g., Gradinger and Ikävalko, 1998; Krembs et al., 2002). The lack of correlation between EPS and DFe, as well as between EPS and  $\text{NH}_4^+$  in our study, does not support this hypothesis, and these processes remain unclear at this stage.

Some studies have reported a conservative behavior of DOC with salinity during ice formation (Giannelli et al., 2001; Amon, 2004), while other studies report elevated stocks of DOC within the ice (e.g., Carlson and Hansell, 2003; Riedel et al., 2008; Zhou et al., 2014). We believe that the extremely low DOC concentrations in seawater in our study led to the low DOC levels observed in newly formed sea ice. The two DOC peaks observed in the ice may be a result of a local solubilization, e.g., destruction of cells incorporated into the ice (Ewert and Deming, 2013).

### 4.3 Incorporation of particulate constituents: Factors influencing enrichment

High EI values for POC, PON, Chl *a*, EPS and PFe indicate that the desalinization processes occurring after initial entrapment in growing sea ice impact dissolved sea salts but not particulate materials. While dissolved sea salts are efficiently flushed out of the ice and rejected to the water column, a disproportionate fraction of particulate materials remain in the ice, possibly attached to the walls of the brine channels.

#### 4.3.1 Growth rate and ice texture

Enrichment indices from our experiments suggest that frazil ice incorporates less POC than columnar ice. The same trend is observed in the natural young ice samples: unconsolidated pancake ice and grey ice showed lower EI values for POC than columnar ice. This trend is contrary to the classical theory of organic matter incorporation into sea ice (scavenging and harvesting; e.g., Reimnitz et al., 1993), but consistent with previous field data where granular ice is not necessarily more enriched than columnar ice (Lannuzel et al., 2014a). The slightly lower POC concentrations found in our samples compared to other studies later in the season (e.g., Lannuzel et al., 2008; Dumont et al., 2009) support observations of seasonal accumulation of POC in Antarctic sea ice.

Furthermore, the relatively high underlying seawater PFe concentrations in our study compared to values measured later in the season support the hypothesis that organic matter and Fe from previous summers can remain in suspension in the water column during autumn (Lannuzel et al., 2010). We note that the PFe (and POC, PON and EPS) concentrations in columnar ice seem to be impacted by the ice-growth rate (Table 2 and Figure S5). We observed a decrease in the PFe concentration between  $T_2$  and  $T_3$  of Exp 1 followed by an increase in PFe between  $T_3$  and  $T_4$ , when the local growth rate increased. This increase in PFe was not observed in Exp 2 where the growth rate remained stable throughout the experiment (Table 2). Less effective rejection of impurities associated with a faster growth rate could explain this observation, but this explanation may need clarification with longer experiments in future. Alternatively, the increase of POC, PON, EPS and PFe in the  $T_4$  core of Exp 1 might reflect the increased influence of 'side-freezing', as evidenced by the thin section of the ice core (Figure S1). 'Side-growth' would likely decrease the efficiency of the gravity-driven brine drainage, resulting in increased bulk ice concentrations. Supporting this inference, the effect is enhanced in Exp 1, where 'side-freezing' started earlier. Also, the combination of vertical and lateral heat sinks might explain the increase in the ice-growth rate observed in the bottom part of the core. Nonetheless, due to the very young age of the ice and the low POC (and Chl *a*) concentrations, we believe that physical incorporation at the very onset of sea-ice formation was the main mechanism responsible for PFe enrichment. Our data suggest that granular ice growth does not incorporate more Fe than columnar ice growth (no general trend in EI values for PFe in granular or columnar ice), confirming previous results in Antarctic pack ice (Lannuzel et al., 2007, 2008, 2014a; van der Merwe et al., 2009).

#### 4.3.2. Biological material: Chl *a* and EPS

Consistent with previous studies of young sea ice (Grossmann and Dieckmann, 1994), *TotChl a* concentrations in both experiments and the sampled natural young sea ice were low. During the experiments, the photoperiod was short (approximately 3.5 hours during Exp 1 and 7 hours during Exp 2) with irradiance not exceeding  $6.9 \text{ W m}^{-2}$  and  $123.4 \text{ W m}^{-2}$  during Exp 1 and 2, respectively. Given this environmental setting, we consider that *in situ* autotrophic growth or increase in intracellular Chl *a* following the incorporation into sea ice (Aguilera et al., 2002) was unlikely. Decreasing *TotChl a*: Phaeopigment ratios from seawater to sea ice (data not shown) support this hypothesis. Peaks of Chl *a* in Exp 1 and 2 could be the result of a combination of contamination by surrounding older ice (i.e., corer not completely vertical when sampling) and a potential effect of spatial patchiness of Chl *a* in the ice and the seawater from which the ice formed (e.g., Meiners et al., 2012). Spatial heterogeneity is inherent to sea ice and was minimized by sampling cores

close to each other (e.g., 0.10 m). Nonetheless, separate cores were needed to obtain sufficient material for analysis of the various parameters.

Sea ice and seawater EPS concentrations were also low compared to previous reports (e.g., Meiners et al., 2004; van der Merwe et al., 2009). Very low EPS production in early spring has been observed together with low biomass when low stress conditions were encountered in Antarctic pack ice (Ugalde et al., 2016). Although concentrations were low, Chl *a* and EPS were both enriched in the ice.

Unlike previous studies (Krembs and Engel, 2001; Meiners et al., 2003; Riedel et al., 2006), EPS did not correlate positively with either Chl *a* or bacteria, suggesting that the EPS in young ice measured in this study did not originate from production in the ice. Exopolymers can form abiotically from dissolved precursors (Passow, 2002; Orellana et al., 2011). Combined processes of low biomass and the absence of EPS precursors, such as DOC, could explain the low EPS concentrations encountered in our study. Also, Riedel et al. (2007) suggested that during the winter period, sea-ice EPS may be broken down or change chemically so that these EPS would not be detected by the AB method. We conclude that in our study, only abiotic processes were responsible for EPS enrichment in sea ice, leading to relatively low enrichment compared to previous studies where biotic and abiotic processes acted in combination (Meiners et al., 2003; Riedel et al., 2007).

#### 4.3.3. Size of the particles

Overall, dissolved components were much less enriched in the ice than the particulate components, with bigger cells (or aggregated cells) showing particularly high enrichment indices (Table 3). This trend has been observed in Arctic sea ice (Gradinger and Ikävalko, 1998; von Quillfeldt et al., 2003; Riedel et al., 2007) and has also been reported from an Antarctic fast ice study, where 97% of Fe incorporated in sea ice was in the form of PFe (Lannuzel et al., 2014b). In their study, large particles (> 10 µm) represented 80% of the PFe pool, indicating that the size of the particles is important.

The higher EI for large autotrophs compared to smaller autotrophs suggests that the size of the algae, or potential chain formation and aggregation, is a key factor in enrichment of autotrophs within sea ice. Preferential incorporation of algae ≥ 5 µm has been reported previously (Gradinger and Ikävalko 1998; Riedel et al., 2007) and cell-associated EPS may contribute to the selection of large autotrophs during sea-ice formation (Gradinger and Ikävalko, 1998).

#### 4.3.4. Role of organic ligands

It has been shown that dissolved organic ligands (e.g., EPS) control the concentration of DFe and maintain it at threshold concentrations in natural Antarctic sea ice (Lannuzel et al., 2015). This mechanism is also potentially the case in our ice-growth experiments, with low EPS concentrations in our samples leading to aggregation/precipitation of DFe into PFe. The potential and multiple roles that EPS play in the incorporation of dissolved and particulate matter into sea ice clearly require further investigation (Lannuzel et al., 2015).

### 4.4 Decoupling between PFe and DFe, and POC and PON during ice growth

A decoupling between the PFe and DFe pools has been observed during the melting of sea ice (van der Merwe et al., 2011a). Our study shows a decoupling between PFe and DFe in the early stage of sea-ice formation, therefore suggesting a decoupling between the two fractions throughout the entire year. During ice formation, and assuming absence of biological activity, the PFe:DFe ratio in ice and seawater should be similar unless these two size fractions are incorporated into the ice differently. Higher ratios in the ice, in both experiments and the natural samples, demonstrate that the sea ice is more enriched in PFe compared to DFe during the early stages of its formation. One way to explain this increase in PFe would be preferential retention of the particulate fraction during brine convection. Also, since brine convection remains active within the skeletal layer during ice growth (Notz and Worster, 2008, 2009), it provides both a continuous input of Fe to the brine system and selective return of DFe to the underlying seawater. Supporting this scenario is the fact that the grey ice sample, the thinnest of our dataset, is the one displaying the highest PFe, DFe and EPS concentrations. We could be witnessing the importance of EPS in scavenging PFe (and DFe) at the very early stages of ice formation. Lowest concentrations in thicker samples could be the result of a 'dilution' compared to what we observed at the sea ice/seawater interface.

A similar decoupling was observed for POC and PON, with POC:PON lower than Redfield in the seawater and above Redfield in the ice (Figure S2). This decoupling could indicate a preferential incorporation of particulate carbon in sea ice relative to particulate nitrogen. EPS C:N ratios lie above the Redfield ratio (Riedel et al., 2007; Niemi and Michel, 2015). The slight enrichment in EPS in the ice is therefore considered to contribute to this change in C:N ratios. The time scales during which both experiments were conducted and the age of the natural sea ice are indeed very short to induce any changes in the phytoplankton/sea-ice algal community and metabolism leading to a modification of the C:N ratio. Decoupling of DOC and DON has been previously observed (e.g., Thomas et al., 2001; Krell et al., 2003; Papadimitriou et al., 2007), but to our knowledge, this is the first time a decoupling of POC and PON has been reported.

## 5. Conclusion

Our results show that only physical processes lead to the enrichment of particles and DFe in the very early stages of ice formation. The size of the particles plays a key role, with larger particles being preferentially enriched in sea ice. Combined with previous studies, the observed decoupling of PFe and DFe when trapped in the ice suggest a decoupling between PFe and DFe throughout the whole year. Our study is unique in its specific dedication to understanding the incorporation processes of Fe into newly formed sea ice, which are critical to understand in a changing sea ice environment. However, a few key questions remain open: what, specifically, is the role of EPS and organic ligands in the incorporation of Fe into sea ice, and what is the impact of ice-growth rate on these enrichment processes? The next steps towards improving understanding would be through the combination of controlled laboratory studies of sea-ice growth under varying initial conditions, small-scale studies of location and characterization of particulate matter within the sea-ice microstructure, and Fe-based biogeochemical modelling for sea ice.

## References

- Aguilera J, Bischof K, Karsten U, Hanelt D, Wiencke C. 2002. Seasonal variation in ecophysiological patterns in macroalgae from an Arctic fjord. II. Pigment accumulation and biochemical defence systems against high light stress. *Mar Biol* 140(6): 1087–1095. doi: 10.1007/s00227-002-0792-y.
- Amon RMW. 2004. The role of dissolved organic matter for the carbon cycle in the Arctic Ocean, in Stein R, Macdonald RW, eds., *The Organic Carbon Cycle in the Arctic Ocean*. Berlin: Springer: pp. 83–99.
- Arar EJ, Collins GB. 1997. Method 445.0: In vitro determination of chlorophyll *a* and pheophytin *a* in marine and freshwater algae by fluorescence. Cincinnati: Office of Research and Development, U.S. Environmental Protection Agency. #445.0.
- Arrigo KR. 2014. Sea ice ecosystems. *Ann Rev Mar Sci* 6: 439–467. doi: 10.1146/annurev-marine-010213-135103.
- Becquevoort S, Dumont I, Tison J-L, Lannuzel D, Sauvée M-L, et al. 2009. Biogeochemistry and microbial community composition in sea ice and underlying seawater off east Antarctica during early spring. *Polar Biol* 32(6): 879–895. doi: 10.1007/s00300-009-0589-2.
- Bowie AR, Townsend AT, Lannuzel D, Remenyi TA, van der Merwe P. 2010. Modern sampling and analytical methods for the determination of trace elements in marine particulate material using magnetic sector inductively coupled plasma-mass spectrometry. *Anal Chim Acta* 676: 15–27. doi: 10.1016/j.aca.2010.07.037.
- Carlson CA, Hansell DA. 2003. The contribution of dissolved organic carbon and nitrogen to the biogeochemistry of the Ross sea, in Ditullio GR, Dunbar RB, eds., *Biogeochemistry of the Ross Sea, Antarctic Research Series*. Washington, D. C.: American Geophysical Union: pp. 123–142. doi: 10.1029/078ars08.
- Cohen J. 1988. *Statistical Power Analysis for the Behavioral Sciences*. 2<sup>nd</sup> ed. New York, USA: Lawrence Erlbaum Associates.
- Cox GFN, Weeks WF. 1975. Brine drainage and initial salt entrapment in sodium chloride ice. *CFREL-RR-345*. Hanover, N.H.: U.S. Army Corps of Engineers Cold Regions Research & Engineering Laboratory.
- Cox GFN, Weeks WF. 1988. Numerical simulations of the profile properties of undeformed first-year sea ice during the growth season. *J Geophys Res-Ocean* 93(C10): 12449–12460. doi: 10.1029/JC093iC10p12449.
- Cutter G, Andersson P, Codispoti L, Croot P, Francois R, et al. 2010. Sampling and sample-handling protocols for GEO-TRACES cruises. <http://www.geotraces.org/libraries/documents/Intercalibration/Cookbook.pdf>.
- de Baar HJW, Timmermans KR, Laan P, De Porto HH, Ober S, et al. 2008. Titan: A new facility for ultraclean sampling of trace elements and isotopes in the deep oceans in the international Geotraces program. *Mar Chem* 111: 4–21. doi: 10.1016/j.marchem.2007.07.009.
- de Jong J, Schoemann V, Maricq N, Mattielli N, Langhorne P, et al. 2013. Iron in land-fast sea ice of McMurdo Sound derived from sediment resuspension and wind-blown dust attributes to primary productivity in the Ross Sea, Antarctica. *Mar Chem* 157: 24–40. doi: 10.1016/j.marchem.2013.07.001.
- de Jong JTM, den Das J, Bathmann U, Stoll MHC, Kattner G, et al. 1998. Dissolved iron at subnanomolar levels in the Southern Ocean as determined by ship-board analysis. *Anal Chim Acta* 377: 113–124. doi: 10.1016/S0003-2670(98)00427-9.
- de Jong JTM, Stammerjohn SE, Ackley SF, Tison J-L, Mattielli N, et al. 2015. Sources and fluxes of dissolved iron in the Bellingshausen Sea (West Antarctica): The importance of sea ice, icebergs and the continental margin. *Mar Chem* 177: 518–535. doi: 10.1016/j.marchem.2015.08.004.
- Dethleff D. 2005. Entrainment and export of Laptev Sea ice sediments, Siberian Arctic. *J Geophys Res-Ocean* 110(7): C07009. doi: 10.1029/2004JC002740.
- Dethleff D, Kempema EW. 2007. Langmuir circulation driving sediment entrainment into newly formed ice: Tank experiment results with application to nature (Lake Hattie, United States; Kara Sea, Siberia). *J Geophys Res-Ocean* 112(C2): C02004. doi: 10.1029/2005JC003259.
- Dethleff D, Kempema EW, Koch R, Chubarenko I. 2009. On the helical flow of Langmuir circulation - Approaching the process of suspension freezing. *Cold Reg Sci Technol* 56(1): 50–57. doi: 10.1016/j.coldregions.2008.10.002.
- Dethleff D, Kuhlmann G. 2009. Entrainment of fine-grained surface deposits into new ice in the southwestern Kara Sea, Siberian Arctic. *Cont Shelf Res* 29(4): 691–701. doi: 10.1016/j.csr.2008.11.009.
- Dieckmann GS, Lange MA, Ackley SF, Jennings Jr JC. 1991. The nutrient status in sea ice of the Weddell Sea during winter: Effects of sea ice texture and algae. *Polar Biol* 11(7): 449–456. doi: 10.1007/bf00233080.
- Dumont I, Schoemann V, Lannuzel D, Chou L, Tison J-L, et al. 2009. Distribution and characterization of dissolved and particulate organic matter in Antarctic pack ice. *Polar Biol* 32(5): 733–750. doi: 10.1007/s00300-008-0577-y.
- Ewert M, Deming JW. 2011. Selective retention in saline ice of extracellular polysaccharides produced by the cold-adapted marine bacterium *Colwellia psychrerythraea* strain 34H. *Ann Glaciol* 52(57): 111–117. doi: 10.3189/172756411795931868.

- Ewert M, Deming JW. 2013. Sea ice microorganisms: Environmental constraints and extracellular responses. *Biology* 2(2): 603–628. doi: 10.3390/biology2020603.
- Garrison DL, Close AR, Reimnitz E. 1989. Algae concentrated by frazil ice: Evidence from laboratory experiments and field measurements. *Antarct Sci* 1(4): 313–316. doi: 10.1017/S0954102089000477.
- Giannelli V, Thomas DN, Haas C, Kattner G, Kennedy H, et al. 2001. Behaviour of dissolved organic matter and inorganic nutrients during experimental sea-ice formation. *Ann Glaciol* 33(1): 317–321. doi: 10.3189/172756401781818572.
- Golden KM, Ackley SF, Lytle VI. 1998. The percolation phase transition in sea ice. *Science* 282: 2238–2241. doi: 10.1126/science.282.5397.2238.
- Gradinger R, Ikävalko J. 1998. Organism incorporation into newly forming Arctic sea ice in the Greenland Sea. *J Plankton Res* 20(5): 871–886. doi: 10.1093/plankt/20.5.871.
- Grasshoff K, Kremling K, Ehrhardt M. 1999. *Methods of Seawater Analysis*. 3<sup>rd</sup> ed. Germany: Wiley-VCH.
- Gross GW. 2003. Nitrates in ice: Uptake; dielectric response by the layered capacitor method. *Can J Phys* 81: 439–450. doi: 10.1139/p02-143.
- Grossmann S, Dieckmann GS. 1994. Bacterial standing stock, activity, and carbon production during formation and growth of sea ice in the Weddell Sea, Antarctica. *Appl Environ Microbiol* 60(8): 2746–2753.
- Grotti M, Soggia F, Ianni C, Frache R. 2005. Trace metals distributions in coastal sea ice of Terra Nova Bay, Ross Sea, Antarctica. *Antarct Sci* 17(2): 289–300. doi: 10.1017/s0954102005002695.
- Hölemann JA, Schirmacher M, Prange A. 1997. Dissolved and particulate major and trace elements in newly formed ice from the Laptev Sea (Transdrift III, October 1995), in Kassens H, Bauch HA, Dmitrenko I, Eicken H, Hubberten H-W, et al., eds. *Land-ocean systems in the Siberian Arctic: Dynamics and history*. Berlin: Springer-Verlag: pp. 101–111.
- Kanna N, Toyota T, Nishioka J. 2014. Iron and macro-nutrient concentrations in sea ice and their impact on the nutritional status of surface waters in the southern Okhotsk Sea. *Prog Oceanogr* 126: 44–57. doi: 10.1016/j.pocean.2014.04.012.
- Knopf DA, Alpert PA, Wang B, Aller JY. 2011. Stimulation of ice nucleation by marine diatoms. *Nat Geosci* 4(2): 88–90. doi: 10.1038/ngeo1037.
- Krell A, Ummerhofer C, Kattner G, Naumov A, Evans D, et al. 2003. The biology and chemistry of land fast ice in the White Sea, Russia - A comparison of winter and spring conditions. *Polar Biol* 26(11): 707–719. doi: 10.1007/s00300-003-0543-7.
- Krems C, Eicken H, Junge K, Deming JW. 2002. High concentrations of exopolymeric substances in Arctic winter sea ice: Implications for the polar ocean carbon cycle and cryoprotection of diatoms. *Deep-Sea Res Pt I* 49(12): 2163–2181. doi: 10.1016/S0967-0637(02)00122-X.
- Krems C, Engel A. 2001. Abundance and variability of microorganisms and transparent exopolymer particles across the ice-water interface of melting first-year sea ice in the Laptev Sea (Arctic). *Mar Biol* 138(1): 173–185. doi: 10.1007/s002270000396.
- Lancelot C, de Montety A, Goosse H, Becquevort S, Schoemann V, et al. 2009. Spatial distribution of the iron supply to phytoplankton in the Southern Ocean: A model study. *Biogeosciences* 6(12): 2861–2878. doi: 10.5194/bg-6-2861-2009.
- Lange MA, Ackley SF, Wadhams P, Dieckmann GS, Eicken H. 1989. Development of sea ice in the Weddell Sea. *Ann Glaciol* 12: 92–96.
- Langway CC. 1958. *Ice fabrics and the universal stage*. Illinois: U.S. Army Snow Ice and Permafrost Research Establishment.
- Lannuzel D, Chever F, van der Merwe PC, Janssens J, Roukaerts A, et al. 2014a. Iron biogeochemistry in Antarctic pack ice during SIPEX-2. *Deep-Sea Res Pt II*: in press. doi: 10.1016/j.dsr2.2014.12.003.
- Lannuzel D, de Jong J, Schoemann V, Trevena A, Tison J-L, et al. 2006. Development of a sampling and flow injection analysis technique for iron determination in the sea ice environment. *Anal Chim Acta* 556: 476–483. doi: 10.1016/j.aca.2005.09.059.
- Lannuzel D, Grotti M, Abelloschi ML, van der Merwe P. 2015. Organic ligands control the concentrations of dissolved iron in Antarctic sea ice. *Mar Chem* 174: 120–130. doi: 10.1016/j.marchem.2015.05.005.
- Lannuzel D, Schoemann V, de Jong J, Chou L, Delille B, et al. 2008. Iron study during a time series in the western Weddell pack ice. *Mar Chem* 108(1–2): 85–95. doi: 10.1016/j.marchem.2007.10.006.
- Lannuzel D, Schoemann V, de Jong J, Pasquer B, van der Merwe P, et al. 2010. Distribution of dissolved iron in Antarctic sea ice: Spatial, seasonal, and inter-annual variability. *J Geophys Res* 115(G3): G03022. doi: 10.1029/2009JG001031.
- Lannuzel D, Schoemann V, de Jong J, Tison J-L, Chou L. 2007. Distribution and biogeochemical behaviour of iron in the East Antarctic sea ice. *Mar Chem* 106(1–2): 18–32. doi: 10.1016/j.marchem.2006.06.010.
- Lannuzel D, Schoemann V, Dumont I, Content M, de Jong J, et al. 2013. Effect of melting Antarctic sea ice on the fate of microbial communities studied in microcosms. *Polar Biol* 36(10): 1483–1497. doi: 10.1007/s00300-013-1368-7.
- Lannuzel D, van der Merwe PC, Townsend AT, Bowie AR. 2014b. Size fractionation of iron, manganese and aluminium in Antarctic fast ice reveals a lithogenic origin and low iron solubility. *Mar Chem* 161: 47–56. doi: 10.1016/j.marchem.2014.02.006.
- Lemke P, Participants of the ANT-XXIX/6 cruise. 2014. The expedition of the research vessel “Polarstern” to the Antarctic in 2013 (ANT-XXIX/6). *Berichte zur Polar-und Meeresforschung*. Bremerhaven: Helmholtz Gemeinschaft. Reports Polar Mar Res 679.
- Lindemann F. 1998. Sediments in Arctic sea ice - entrainment, characterization and quantification [PhD thesis]. Kiel University, Germany: Mathematisch-Naturwissenschaftliche Fakultät.
- Lindemann F, Hölemann JA, Korabely A, Zachek A. 1997. Particle entrainment into newly forming sea ice - Freeze-up studies in October 1995, in Kassens H, Bauch HA, Dmitrenko IA, Eicken H, Hubberten H-W, et al., eds., *Land-ocean systems in the Siberian Arctic: Dynamics and history*. Berlin: Springer-Verlag: pp. 113–125.
- Lizotte MP. 2003. The microbiology of sea ice, in Thomas DN, Dieckmann GS, eds., *Sea Ice: An introduction to its physics, chemistry, biology and geology*. Blackwell Science: pp. 184–210.
- Martin S, Kauffman P. 1981. A field and laboratory study of wave damping by grease ice. *J Glaciol* 27(96): 283–313.
- Meese DA. 1989. The chemical and structural properties of sea ice in the southern Beaufort sea. *CRREL Report 89-25*. Hanover, N.H.: U.S. Army Corps of Engineers Cold Regions Research & Engineering Laboratory.

- Meiners K, Brinkmeyer R, Granskog MA, Lindfors A. 2004. Abundance, size distribution and bacterial colonization of exopolymer particles in Antarctic sea ice (Bellingshausen Sea). *Aquat Microb Ecol* **35**: 283–296. doi: 10.3354/ame035283.
- Meiners K, Gradinger R, Fehling J, Civitarese G, Spindler M. 2003. Vertical distribution of exopolymer particles in sea ice of the Fram Strait (Arctic) during autumn. *Mar Ecol-Prog Ser* **248**: 1–13. doi: 10.3354/meps248001.
- Meiners KM, Vancoppenolle M, Thanassekos S, Dieckmann GS, Thomas DN, et al. 2012. Chlorophyll *a* in Antarctic sea ice from historical ice core data. *Geophys Res Lett* **39**(21): L21602. doi: 10.1029/2012GL053478.
- Müller S, Vähätalo AV, Stedmon CA, Granskog MA, Norman L, et al. 2013. Selective incorporation of dissolved organic matter (DOM) during sea ice formation. *Mar Chem* **155**: 148–157. doi: 10.1016/j.marchem.2013.06.008.
- Niemi A, Michel C. 2015. Temporal and spatial variability in sea-ice carbon: Nitrogen ratios on Canadian Arctic shelves. *Elem Sci Anth* **3**: 000078. doi: 10.12952/journal.elementa.000078.
- Notz D, Worster MG. 2008. In situ measurements of the evolution of young sea ice. *J Geophys Res-Ocean* **113**(C3): C03001. doi: 10.1029/2007JC004333.
- Notz D, Worster MG. 2009. Desalination processes of sea ice revisited. *J Geophys Res-Ocean* **114**(C5): C05006. doi: 10.1029/2007JC004333.
- Nürnberg D, Wollenburg I, Dethleff D, Eicken H, Kassens H, et al. 1994. Sediments in Arctic sea ice: Implications for entrainment, transport and release. *Mar Geol* **119**(3–4): 185–214. doi: 10.1016/0025-3227(94)90181-3.
- Obata H, Karatani H, Nakayama E. 1993. Automated determination of iron in seawater by chelating resin concentration and chemiluminescence detection. *Anal Chem* **65**(11): 1524–1528. doi: 10.1021/ac00059a007.
- Orellana MV, Matrai PA, Leck C, Rauschenberg CD, Lee AM, et al. 2011. Marine microgels as a source of cloud condensation nuclei in the high Arctic. *P Natl Acad Sci* **108**(33): 13612–13617. doi: 10.1073/pnas.1102457108.
- Osterkamp TE, Gosink JP. 1983. Frazil ice formation and ice cover development in interior Alaska streams. *Cold Reg Sci Technol* **8**(1): 43–56. doi: 10.1016/0165-232X(83)90016-2.
- Palmisano AC, Garrison DL. 1993. Microorganisms in Antarctic sea ice, in Friedmann EI, ed., *Antarctic Microbiology*. New-York: Wiley: pp. 167–218.
- Papadimitriou S, Thomas DN, Kennedy H, Haas C, Kuosa H, et al. 2007. Biogeochemical composition of natural sea ice brines from the Weddell Sea during early austral summer. *Limnol Oceanogr* **52**(2): 1809–1823. doi: 10.4319/lo.2007.52.5.1809.
- Passow U. 2002. Transparent exopolymer particles (TEP) in aquatic environments. *Prog Oceanogr* **55**(3): 287–333. doi: 10.1016/s0079-6611(02)00138-6.
- Passow U, Alldredge AL. 1995. A dye-binding assay for the spectrophotometric measurement of transparent exopolymer particles (TEP). *Limnol Oceanogr* **40**: 1326–1335. doi: 10.4319/lo.1995.40.7.1326.
- Petrich C, Eicken H. 2010. Growth, structure and properties of sea ice, in Thomas DN, Dieckmann GS, eds., *Sea Ice*. 2<sup>nd</sup> ed. Oxford: Wiley-Blackwell: pp. 23–77.
- Qian J, Mopper K. 1996. Automated high-performance, high-temperature combustion total organic carbon analyzer. *Anal Chem* **68**(18): 3090–3097. doi: 10.1021/ac960370z.
- Reimnitz E, Clayton JR, Kempema EW, Payne JR, Weber WS. 1993. Interaction of rising frazil with suspended particles: Tank experiments with applications to nature. *Cold Reg Sci Technol* **21**(2): 117–135. doi: 10.1016/0165-232X(93)90002-P.
- Riedel A, Michel C, Gosselin M. 2006. Seasonal study of sea-ice exopolymeric substances on the Mackenzie shelf: Implications for transport of sea-ice bacteria and algae. *Aquat Microb Ecol* **45**(2): 195–206. doi: 10.3354/ame045195.
- Riedel A, Michel C, Gosselin M, LeBlanc B. 2007. Enrichment of nutrients, exopolymeric substances and microorganisms in newly formed sea ice on the Mackenzie shelf. *Mar Ecol-Prog Ser* **342**: 55–67. doi: 10.3354/meps342055.
- Riedel A, Michel C, Gosselin M, LeBlanc B. 2008. Winter–spring dynamics in sea-ice carbon cycling in the coastal Arctic Ocean. *J Mar Syst* **74**(3–4): 918–932. doi: 10.1016/j.jmarsys.2008.01.003.
- Rintala J-M, Piiparinen J, Blomster J, Majavena M, Müller S, et al. 2014. Fast direct melting of brackish sea-ice samples results in biologically more accurate results than slow buffered melting. *Polar Biol* **37**: 1811–1822. doi: 10.1007/s00300-014-1563-1.
- Rózańska M, Poulin M, Gosselin M. 2008. Protist entrapment in newly formed sea ice in the coastal Arctic Ocean. *J Mar Syst* **74**(3–4): 887–901. doi: 10.1016/j.jmarsys.2007.11.009.
- Schoemann VS, de Jong JTM, Lannuzel D, Tison J-L, Delille B, et al. 2008. Microbiological control on the cycling of Fe and its isotopes in Antarctic sea ice. *Geochim Cosmochim Acta* **72**(12): A837.
- Sedwick PN, DiTullio GR. 1997. Regulation of algal blooms in Antarctic shelf waters by the release of iron from melting sea ice. *Geophys Res Lett* **24**(20): 2515–2518. doi: 10.1029/97GL02596.
- Smedsrud LH. 1998. Estimating aggregation between suspended sediments and frazil ice. *Geophys Res Lett* **25**(20): 3875–3878. doi: 10.1029/1998GL900051.
- Spindler M. 1994. Notes on the biology of sea ice in the Arctic and Antarctic. *Polar Biol* **14**(5): 319–324. doi: 10.1007/BF00238447.
- Thomas DN, Kattner G, Engbrodt R, Giannelli V, Kennedy H, et al. 2001. Dissolved organic matter in Antarctic sea ice. *Ann Glaciol* **33**(1): 297–303. doi: 10.3189/172756401781818338.
- Thomas DN, Papadimitriou S, Michel C. 2010. Biogeochemistry of sea ice, in Thomas DN, Dieckmann GS, eds., *Sea Ice*. 2<sup>nd</sup> ed. Oxford: Wiley-Blackwell: pp. 425–467.
- Ugalde SC, Westwood KJ, Van Den Enden R, McMinn A, Meiners KM. 2016. Characteristics and primary productivity of East Antarctic pack ice during the winter–spring transition. *Deep-Sea Res Pt II: in press*. doi: 10.1016/j.dsr2.2015.12.013.
- Vancoppenolle M, Goosse H, de Montety A, Fichefet T, Tremblay B, et al. 2010. Modeling brine and nutrient dynamics in Antarctic sea ice: The case of dissolved silica. *J Geophys Res-Ocean* **115**(C2): C02005. doi: 10.1029/2009JC005369.
- van der Merwe P, Lannuzel D, Bowie AR, Mancuso Nichols CA, Meiners KM. 2011a. Iron fractionation in pack and fast ice in East Antarctica: Temporal decoupling between the release of dissolved and particulate iron during spring melt. *Deep-Sea Res Pt II* **58**(9–10): 1222–1236. doi: 10.1016/j.dsr2.2010.10.036.
- van der Merwe P, Lannuzel D, Bowie AR, Meiners KM. 2011b. High temporal resolution observations of spring fast ice melt and seawater iron enrichment in East Antarctica. *J Geophys Res* **116**(G3): G03017. doi: 10.1029/2010JG001628.

- van der Merwe P, Lannuzel D, Mancuso Nichols CA, Meiners K, Heil P, et al. 2009. Biogeochemical observations during the winter–spring transition in East Antarctic sea ice: Evidence of iron and exopolysaccharide controls. *Mar Chem* 115(3–4): 163–175. doi: 10.1016/j.marchem.2009.08.001.
- von Quillfeldt CH, Ambrose Jr WG, Clough LM. 2003. High number of diatom species in first-year ice from the Chukchi Sea. *Polar Biol* 26(12): 806–818. doi: 10.1007/s00300-003-0549-1.
- Wang S, Bailey D, Lindsay K, Moore JK, Holland M. 2014. Impacts of sea ice on the marine iron cycle and phytoplankton productivity. *Biogeosciences* 11(17): 4713–4731. doi: 10.5194/bg-11-4713-2014.
- Weeks W, Ackley SF. 1982. The growth, structure, and properties of sea ice. *Monog. 82-1*. Hanover, N.H.: U.S. Army Corps of Engineers Cold Regions Research & Engineering Laboratory.
- Weeks WF. 2010. *On sea ice*. Fairbanks: University of Alaska Press.
- Weissenberger J, Grossmann S. 1998. Experimental formation of sea ice: Importance of water circulation and wave action for incorporation of phytoplankton and bacteria. *Polar Biol* 20(3): 178–188. doi: 10.1007/s003000050294.
- Westerlund S, Öhman P. 1991. Iron in the water column of the Weddell Sea. *Mar Chem* 35(1-4): 199–217. doi: 10.1016/S0304-4203(09)90018-4.
- Zhou J, Delille B, Eicken H, Vancoppenolle M, Brabant F, et al. 2013. Physical and biogeochemical properties in landfast sea ice (Barrow, Alaska): Insights on brine and gas dynamics across seasons. *J Geophys Res-Ocean* 118: 3172–3189. doi: 10.1002/jgrc.20232.
- Zhou J, Delille B, Kaartokallio H, Kattner G, Kuosa H, et al. 2014. Physical and bacterial controls on inorganic nutrients and dissolved organic carbon during a sea ice growth and decay experiment. *Mar Chem* 166: 59–69. doi: 10.1016/j.marchem.2014.09.013.

#### Contributions

- Contributed to conception and design: JJ, KMM, DL
- Contributed to acquisition of data: JJ, BD, GD, JLT
- Contributed to analysis and interpretation of data: JJ, JLT, BD, GD, KMM, DL
- Drafted and revised the article: JJ, KMM, JLT, GD, BD, DL
- Approved the submitted version for publication: JJ, KMM, DL, JLT, GD, BD

#### Acknowledgments

The authors thank the officers and crew of the R.V *Polarstern* for their logistical support during the cruise. We thank Peter Lemke for overall organization of the Antarctic Winter Ecosystem and Climate Study (AWECS). We are grateful to Jeroen de Jong for his help in the field when setting up the *in situ* experiments. We thank Anne-Mari Luhtanen for providing the bacterial counts for this study and Pier van der Merwe for assistance in the lab with the FIA. Many thanks to the two anonymous reviewers for their valuable comments and suggestions that considerably improved this manuscript. We also thank Jody Deming, chief editor of the Ocean Science domain of *Elementa*, and Lisa Miller, associate editor of the Special Feature BEPSII, for their thorough reviews of this manuscript. This is a contribution to SCOR WG 140 on Biogeochemical Exchange Processes at Sea Ice Interfaces (BEPSII).

#### Funding information

This work was funded by the Australian Research Council (LE0989539 and DE120100030) and the Australian Government Cooperative Research Centres Programme through the Antarctic Climate & Ecosystems Cooperative Research Centre (ACE CRC) as well as through the Belgian Science Policy (BELSPO) through the Bigsouth project (SD/CA/05A). BD is a research associate of the Fonds de la Recherche Scientifique – FNRS. The work contributes to the Quantitative Antarctic Science Program jointly led by the University of Tasmania and the Australian Antarctic Division.

#### Competing interests

The authors declare they have no competing interest of any kind with this research and the publication of this manuscript.

#### Supplemental material

- **Figure S1. Ice texture for Exp 1 and 2.**  
Ice texture for a) Exp 1 and b) Exp 2 for each time step. The black bar represents the granular ice and the grey bar the columnar ice. Total ice thickness (in m) and time steps ( $T_1$ – $T_4$ ) are indicated.  
doi: 10.12952/journal.elementa.000123.s001
- **Figure S2. Particulate organic carbon and nitrogen concentrations and POC:PON ratio in ice and seawater.**  
Concentrations of particulate organic carbon (POC, grey bars, in  $\mu\text{mol L}^{-1}$ ) and particulate organic nitrogen (PON, white bars, in  $\mu\text{mol L}^{-1}$ ) in the ice and the seawater for each time step ( $T_1$ – $T_4$ ) during a) Exp 1 and b) Exp 2 and in c) the natural young ice samples. The black dots are the molar POC:PON ratios. In the natural ice samples, the seawater concentration is the mean of each seawater concentration corresponding to the different ice samples ( $n = 5$ ). The error bars correspond to the standard deviation of the seawater concentrations ( $n = 5$ ). Sw refers to seawater, Uncons. pcke. to unconsolidated pancake, Semi-cons. pcke. to semi-consolidated pancake, and Cons. pcke. to consolidated pancake.  
doi: 10.12952/journal.elementa.000123.s002
- **Figure S3. Extracellular polymeric substances and total Chl *a* concentrations in ice and seawater.**  
Extracellular polymeric substances (EPS) concentrations (grey bars, in  $\mu\text{g eq L}^{-1}$ ) and total Chl *a* concentration (*Total Chl a*, black dots, in  $\mu\text{g L}^{-1}$ ) in the ice and the seawater for each time step ( $T_1$ – $T_4$ ) during a) Exp 1 and b) Exp 2 and in c) the natural young ice samples. The *Total Chl a* concentration in seawater during Exp 1 was below the detection limit. In the natural ice samples, the seawater concentration is the mean of each seawater concentration corresponding to the different ice samples ( $n = 5$ ). The error bars correspond to the standard deviation of the seawater concentrations ( $n = 5$ ). Sw refers to seawater, Uncons. pcke. to unconsolidated pancake, Semi-cons. pcke. to semi-consolidated pancake, and Cons. pcke. to consolidated pancake.  
doi: 10.12952/journal.elementa.000123.s003

- **Figure S4. Bacterial count in ice and seawater for the *in situ* ice-growth experiments.** Bacteria concentration (in cells mL<sup>-1</sup>) in seawater and ice for each time step (T<sub>1</sub>-T<sub>4</sub>) during Exp 1 (grey bars) and Exp 2 (white bars).  
doi: 10.12952/journal.elementa.000123.s004
- **Figure S5. Particulate and dissolved iron concentrations and PFe:DFe ratio in sea ice and seawater.** Particulate Fe (PFe) concentrations (grey bars, in nmol L<sup>-1</sup>), dissolved Fe (DFe) concentrations (white bars, in nmol L<sup>-1</sup>) and PFe:DFe ratio (black dots) in the ice and the seawater for each time step (T<sub>1</sub>-T<sub>4</sub>) during a) Exp 1 and b) Exp 2 and in c) the natural young ice samples. In the natural ice samples, the seawater concentration is the mean of each seawater concentration corresponding to the different ice samples (n = 4). The error bars correspond to the standard deviation of the seawater concentrations (n = 4). No iron data (ND) are available for the unconsolidated pancake. Sw refers to seawater, Uncons. pcke. to unconsolidated pancake, Semi-cons. pcke. to semi-consolidated pancake, and Cons. pcke. to consolidated pancake.  
doi: 10.12952/journal.elementa.000123.s005
- **Figure S6. Ice texture for the natural young ice samples.** Ice texture and ice thickness (in m) of the natural young ice at a) unconsolidated pancake station 486, b) semi-consolidated pancake station 488 and c) consolidated pancake station 489. The black bar represents the granular ice and the grey bar the columnar ice. Note that the entire core is represented here while only the bottom part of the core has been analyzed for biogeochemical parameters.  
doi: 10.12952/journal.elementa.000123.s006

#### Data accessibility statement

All data will be available at the PANGAEA, Data Publisher for Earth & Environmental Science

#### Copyright

© 2016 Janssens et al. This is an open-access article distributed under the terms of the Creative Commons Attribution License, which permits unrestricted use, distribution, and reproduction in any medium, provided the original author and source are credited.